Authors' response to reviews for Manuscript esurf-2018-65

"How steady are steady-state mountain belts? - a re-examination of the Olympic Mountains (Washington State, USA)"

By: Michel et al.

Dear Editor,

We acknowledge the time and effort the associate handling editor as well as the two reviewers have put into handling and reviewing our manuscript. The manuscript benefited significantly from the suggestions by the reviewers and we hope we sufficiently addressed the concerns of the reviewers. Based on their suggestions, we made changes to the entire manuscript, and particularly rewrote and reformulated the introduction, the methods section as well as the discussion, where we also included a new section (Section 5.5). Furthermore, we conducted additional model simulations and provide the results from these in the electronic supplement.

In the following, we identify the five main concerns raised by the reviewers and we briefly describe, how we addressed these. After this the point-by-point response to both reviewers can be found. This response includes our two comments already posted online during the discussion period of the paper, but now also indicates the discrete changes in the revised manuscript. At the end of this letter we provide the revised manuscript in a track-changes fashion, so that the editor and reviewers can readily see, what we changed in this resubmitted version of the manuscript.

The main issues raised by the reviewers partly overlapped. We summarize these below, together with a brief response (a more thorough response is provided in the point-by-point section):

1) Inappropriate modelling strategy for our thermo-kinematic model
   Reviewer#1 advocates that a full 3D model using Pecube would be more appropriate and reviewer#2 suggests to use thermal models like QtQt for our purpose. As we further elaborate in the detailed response below, our "simple" 1D model approach using Pecube with the Monte-Carlo algorithm is most suited for the main purpose: we want to demonstrate that exhumation is temporally variable. Setting up a new full 3D model also considering the observed temporal variations requires to constrain many more parameters (which is partly not possible with the data available at present) and would be a paper on its own.
   In the revised manuscript we rewrote the methods section for the kinematic modeling (Section 3.2) and tried to better explain our purpose in using the 1D model. We also conducted additional model simulations in order to investigate the timestep bias mentioned by reviewer #2, which we report in the electronic supplement of the manuscript.

2) 2D and 3D flux steady-state analysis

Both reviewers suggest to conduct the flux steady-state analysis only either in 2D or 3D. The previous analysis by Batt et al. (2001) was performed in 2D, hence we also provide a 2D analysis, to make results from both studies better comparable. However, as we show, with our approach flux steady-state is only attained using a 3D geometry. This is a new and unexpected observation, which has not been reported for the Olympic Mountains so far.

So, we still kept both the 2D and 3D analysis in the revised paper. However, we try to more clearly convey our purpose for doing so in the revised manuscript. We now explain in detail the approach of Batt et al (2001) in the introduction and how our approach is different. We also emphasize in the introduction and conclusion that the Olympic Mountains are only in steady-state, if a three-dimensional geometry is assumed.

3) Limitations of our approaches

This was particularly a concern raised by reviewer#2. We include a new chapter in the discussion (section 5.5) where we try to address the limitations inherent to our approaches, including thermo-kinematic modeling and parameters affecting our flux steady-state analysis (like sediment thickness and wedge geometry).

4) Pre-Quaternary sediment thickness for influx calculations

Reviewer#1 raised the concern that our value of 1.5 km for the pre-Quaternary sediment thickness used in our influx calculations is not well constrained.

We provide a detailed approach for estimating this difficult to constrain parameter in the electronic supplement of the manuscript (Section S3.2).

5) Novelty of presented results

Reviewer#2 raises the issue whether the outcomes from this work are new compared to the published work of Michel et al. (2018) and Batt et al. (2001).

To overcome this concern, we reformulated the introduction, which now includes a more detailed description of the previous approach of Batt et al. (2001). We now also highlight, which of our results and observations are novel, compared to published work (for instance the observed drop in exhumation rates and that flux steady-state is only attained using a three-dimensional geometry).

In the following we provide the point-by-point response towards the comments made by the reviewers. Note that the line numbers refer to the lines in pdf-version of the revised manuscript.

The reviewers' comments are in italics, **our response is in bold**. Our changes made in the manuscript are highlighted in blue.

Reply to reviewer#1

The manuscript presents new thermochronological data from the Olympic Mountains in Washington State, USA. In addition, the paper presents a quantification of the influx and outflux of material to the mountain range over the last 14 million years, in order to discuss whether this accretionary wedge range is in a flux steady state. The influx of material into the accretionary wedge is based on knowledge from offshore sediment volumes and plate velocities, whereas the outflux is based on an exhumation map from previous thermochronological work in the range.

The topic is interesting and the overall finding represents a new scientific contribution. However, I find it peculiar how the authors present newly obtained data, apparently without using them in the following calculation of the denudation pattern/outflux. As it is presented now, the paper appears quite fragmented, and one wonders what is really gained form including the new data. In this sense, the paper could just as well be split into two separate papers. One on the newly obtained thermochron data, and one on the flux in and out of the range.

We thank the reviewer first for the time she or he has spent on revising the manuscript, and second for acknowledging that the results from this work are new and contribute to this topic. We understand that it seems counterintuitive to present new thermochronometry data and to not include them in the influx and outflux calculations. However, we still use the results obtained from the new data in our qualitative discussion of flux steady-state, where the modeled exhumation histories demonstrate a strong temporal variation in exhumation (equating to a variation in the outflux). However, as discussed in the paper, we can't use these results for our quantitative assessment. We also hesitated to include all of the new data and published data in a new 3D Pecube model for reasons further outlined below.

In the revised manuscript, we will develop the implications of the new data in more detail, so to demonstrate that our findings are stronger with their inclusion (to avoid a splitting into two papers).

We emphasize that only our new thermochronometry data reveal the hitherto unnoticed decrease in exhumation rates in the introduction (lines 83 – 85) and conclusion (lines 707 –

714). We also highlight our purpose of taking new thermochronometry samples in order to reconstruct exhumation in the methods section (lines 208 – 211).

Regarding the flux calculations, more justification is needed for the choice of sediment thickness. It seems like the 1.5 km is taken out of the blue. Also related to this, it should be better explained what the gain is from doing both the 2D and 3D approaches. Why not just do the 3D, and test this with the 2D cross sections? Isn't it obvious that a 2D approach is not ideal when a strong spatial gradient exists in exhumation perpendicular to the 2D section?

These are good and helpful remarks by the reviewer. Indeed, we did not explain in detail why we used 1.5 km as minimum sediment thickness. A more detailed comment on this is provided below and a thorough elaboration on this will be included in the revised manuscript.

This comment highlights that we did not convey clearly enough our approach for performing both a 2D and 3D flux calculation. Our intention with providing both 2D and 3D flux analyses stems from the fact that the previous attempts for estimating the flux balance in the Olympic Mountains were performed in 2D (e.g. Batt et al. 2001). As mentioned by the reviewer, the spatially variable exhumation rates suggest that the outflux in this mountain range is highly variable, depending on the actual position in the mountain range. Therefore, our intention was to perform an analysis with the established 2D setup and to compare this with an analysis based on a 3D geometry and to see whether different outcomes are obtained. As we describe in the manuscript, on long timescales flux steady-state is only achieved using a 3D geometry, whereas the 2D geometry requires unrealistic parameters (or is an oversimplification). We believe, that this is an interesting outcome, given that the previous analysis has been done in 2D.

In the revised manuscript, we will explain in more detail our approach in the methods section and discuss in more detail what is gained from performing both 2D and 3D analyses in section 5.2.

Regarding the concern of the 2D and 3D flux calculations, we rephrased the introduction and try to explain that the previous approach for assessing flux steady-state in the Olympic Mountains was performed in 2D (lines 55 – 61). We highlight that we want to compare results from both 2D and 3D (lines 303 – 309), and finally emphasize that in our case, contrary to the previous publication flux steady-state is only obtained using a three-dimensional geometry (lines 601 – 607 and 723 – 725), showing that the geometry inherent for flux steady-state analysis is important.

Introduction: Lines 56-61: you don't need to summarize the conclusions here in the introduction.

This seems to be a choice of style. Since the manuscript has not reached a space limit, we prefer to leave the introduction as it is.

Methods: 150-153: Would be great to introduce here already what methods are used for the flux calculations.

Thank you for pointing this out, we will insert a brief introduction to our used flux calculations at this section of the revised manuscript.

A brief description of our flux calculations is now given in lines 203 – 205.

182-: Although I appreciate that a 1D approach can give valuable results, I cannot stop to wonder why the authors did not take the full 3D approach, which is the core purpose of Pecube. To the best of my knowledge, all the authors are doing could be done in Pecube in 3D. Using all existing data, they could make an updated exhumation map for the region to be used in their calculations of the outflux. You should as a minimum discuss why it is not feasible to do a full 3D inversion in Pecube.

Indeed, the prime purpose of Pecube is to perform full 3D inversions of thermochronometric datasets. After inspecting our thermochronometric dataset (particularly the samples with multiple thermochronometer systems available), we suspected a possible strong variation in exhumation rates, because of the observed ages (e.g. young AHe ages, overlapping, 5–7 Ma old AFT/ZHe ages). Hence, our prime intention was to evaluate this hypothesis. To perform a full 3D model in Pecube, an exhumation rate pattern, an exhumation history (so temporal variations in exhumation) and also topography need to be prescribed in advance. In the 1D model, thousands of possible exhumation histories are explored with the Monte-Carlo algorithm, yielding a best-fit history for the observed thermochronometer ages for the respective sample. The advantage to this method is that histories with variations in exhumation rates can be robustly constrained (and do not have to be guessed in advance by the modeler in a 3D approach, which could introduce a bias). We use the results obtained by this approach for our qualitative assessment of the flux steady-state, where we argue for temporal variations in the outflux, because also the exhumation rates are temporally variable.

As mentioned by the reviewer, we could use all existing thermochronometric data and use the temporal evolution of exhumation rates obtained from the 1D modeling to set up a 3D model. However, the differences in exhumation rates between the seven samples modeled with 1D (e.g. the timing and magnitudes in variation of exhumation rates) would be difficult to account for in a 3D model, and large misfits between modeled and observed ages would be expected, if all existing thermochronometer ages (from this work, as well as literature) are included in a 3D model. Such misfits could be

expected given that samples are located in different parts of the accretionary wedge, which are probably separated by faults. Setting up a 3D Pecube model with faults on top of the ellipse exhumation rate pattern in order to simulate different parts of the accretionary wedge would be a paper on its own and many additional parameters would need to be constrained. Hence, we did not include a model like this in the current manuscript.

For our quantitative outflux analysis, there would also be no benefit from an updated exhumation map (with an additional temporal variation in exhumation). The integrated amount of exhumation considered during the 14 Myr period (this value is used during the outflux calculations) would still be the same as with the current exhumation rate map (i.e., even a more sophisticated model will still result in the same amount of exhumation).

In the revised manuscript, we will include a more thorough discussion (including the remarks above) about the concerns raised by the reviewer.

We reformulated parts of the methods section on the thermo-kinematic modeling (lines 242 – 290), particularly addressing the poor spatial resolution of the seven samples considered for modeling (lines 280 – 284). In the new limitations section (Section 5.5), we also emphasize that in order to create a new 3D model including all data and considering the observed temporal variations in exhumation would require to constrain parameters like faults, which is not feasible with the data available at present (lines 633 – 644).

220-236: this section could be clearer and more up-front about the 2D vs. 3D approaches. Why not just use the 3D approach? What is gained from the 2D? this should be made clear.

See our response to the reviewer's comment above.

252-255: the use of 1.5 km as the minimum for the previous thickness of offshore sediment is not properly justified. It is stated specifically that this is the largest unknown, and right now it seems you have grabbed this number out of thin air. Could there not have been more sediment earlier where you argue for a much higher exhumation rate?

Thank you for pointing this out. We agree with the reviewer, that the minimum sediment thickness of 1.5 km needs to be better justified. A more thorough way of constraining this parameter is explained in the following, and we will modify the manuscript to explain this better. More specifically, during the entire history of sediment accretion at the deformation front since ~40 Ma, the sediment thickness was likely different from the reported 1.5 km, but to get constraints on the sediment thickness for this entire period is difficult, as most of it has already been incorporated in the accretionary wedge. However, we focus our analysis on the past 14 Myr, where obtaining constraints is

easier. As shown in Figure 3 of the manuscript, the oceanic crust subducted at present is very young (~6–9 Ma). The young age together with the fast subduction rate (which was even faster prior to 6 Ma) prevent the accumulation of a thick succession of sediments on top of the oceanic crust (e.g. the pre-Quaternary sedimentation rates obtained from the ODP boreholes are around 80–110 m/Myr, Table 1). Assuming it takes the oceanic crust about 9 Myr to reach the deformation front (the oldest oceanic crust at the deformation front is currently 9 Ma old) would yield a sediment thickness of ~700–1000 m at the deformation front. However, this is likely an underestimation of the actual thickness, because the inherent assumption for this calculation is that the spreading rate and convergence rate stay constant over time. Furthermore, the sedimentation rate likely increases closer to the deformation front, because more detritus is delivered through submarine canyons and turbidity currents (the ODP boreholes were drilled on the deep sea plain or on a submarine fan ~120 km away from the deformation front, Figure 3). Therefore, using a minimum sediment thickness of 1500 m for pre-Quaternary times should correspond to a good estimation of this otherwise difficult to constrain parameter.

As the reviewer mentions, we observe high exhumation rates at ~6 Ma, which consequently yields a higher sediment supply to the ocean. But the high exhumation rate period is followed by a period of very slow exhumation rates from ~6–2 Ma (Figure 8), so the sediment supply to the ocean will also decrease. Furthermore, the sediment material entering the accretionary wedge at the deformation front is a mixture of material delivered from different sources (e.g. Olympic Mountains, Vancouver Island, Canadian Cordillera). Variations in exhumation rates in these different source regions will also result in variable amounts of sediment from the respective source region, however the effect of these variations on the sediment thickness is difficult to constrain.

A more thorough elaboration on the used sediment thickness will be included in the revised manuscript.

In line 326 – 327 we refer to the revised electronic supplement, which now contains a detailed explanation about the Pre-Quaternary sediment thickness in section S3.1.

Lines 295-298: as mentioned above, it seems odd that you don't want to actually use the data you present here. Either you should use all available data together, or you can just as well leave the new data out.

We understand the concern of the reviewer, to not use the presented data in all of our analyses. As outlined in the comments above, we are unfortunately not able to include the data in a new 3D Pecube model, to obtain an updated exhumation pattern (for the quantitative flux calculations). However, we still use information obtained from the new

data for qualitative flux analysis, clearly showing variations in exhumation rates. The change in exhumation rates at ~6 Ma due to a change in convergence rate is also a new observation, that has previously not been reported for the Olympic Mountains and we will clearly state this in the revised manuscript.

Results: 312-318: I don't see AFT ages mentioned here?

Thank you for indicating this, the AFT ages will be included in the revised manuscript.

The AFT ages of the respective samples are now mentioned in lines 402 – 410.

345: should it not be OP1551 to be consistent with figures?

Indeed, this typo will be corrected in the revised manuscript.

The correct sample ID OP1551 is now given in line 441.

357: I would argue that the volumes vary with the location in the wedge geometry, latitude is irrelevant.

We will consider the suggestion and replace "latitude" in the revised manuscript.

We rephrased latitude with " … depending on the position within the wedge." (line 454 – 455).

Discussion: Lines 378-382. This is unclear. You start with: "In the absence of a strong lateral gradient". . . and end with "due to the strong spatial gradient. . ."

Our intention was to quickly introduce the classic way of interpreting an age-elevation transect (which requires the absence of a lateral gradient in exhumation). However, this is not possible in the Olympic Mountains (due to the spatial gradient in exhumation rates). We will rephrase this paragraph in the revised version of the manuscript, to make it clearer.

This entire section of the discussion was rephrased and the particular paragraph the reviewer is referring to is reformulated (lines 477 – 483) so that it should be better understandable now.

Lines 401-402: references are needed here, or rephrase to avoid passive voice.

References to Michel et al. 2018 and Brandon et al. 1998 will be included in the revised manuscript.

This entire paragraph is now significantly changed, so that we did not have to include references (lines 502 – 511).

Lines 480-482: more likely a lower outflux outside of the profile, is it not?

Thank you for indicating this, we will include this in the revised manuscript.

290 Liens 593 – 594 now address this remark by the reviewer.

Reply to reviewer#2

This paper by Michel et al. aims at assessing the degree of steady-state of the accretionary prism of the Olympic Mountains. The authors used existing and new thermochronological
295 *data, to assess by an inverse model, the evolution of exhumation and denudation during the last 14 Myr that they equate to material outflux. For influx, they consider the rate of plate tectonic convergence multiplied by sediment thickness at the wedge front, and it is implicitly assumed that only frontal accretion contributes to material influx (a largely questionable hypothesis).*

300 *The question addressed by this paper is of interest for a large community, and I thank the authors for the efforts they have put in this manuscript. However:*

We thank the reviewer for his time she or he spent on reviewing our manuscript and that she/he agrees, that this topic is of interest for a large community.

1) The method used (inverse model based on Pecube with only 1D temperature and
305 *discretized at 1 Myr) is not optimal.*

It appears we did not succeed in conveying our main purpose of using this modeling approach. We comment in detail on this concern in our responses below and show how we will address this in the revised manuscript.

2) The influx reconstruction is not constrained or discussed well enough, in particular the
310 *contribution of fluxes other than frontal accretionary fluxes (such as isostasy, etc) or temporal changes in the structure of the wedge are not inferred*.

These are interesting remarks that definitely need to be addressed. We provide a more detailed response in the comments below.

3) The paper is sometimes confusing (e.g., some thermochronological data are not all used in the inversion, the 2D or 3D accretionary fluxes are not necessary (only in 3D or in 2D)).

Thank you for pointing this out. We only used the thermochronometry data from seven samples in our modeling, because these seven samples are multi-chronometer samples, so that three or four thermochronometer systems (AHe, AFT, ZHE, ZFT) are available for each sample. We omitted the remaining samples, because for these only one or two thermochronometer systems are available (e.g. AHe and ZHe) or most of the thermochronometer systems are unreset. Hence the seven considered samples yield the best-constrained exhumation histories. Relying on these specific samples provides the most consistent framework for equal comparison of exhumation histories across the range.

Our purpose for providing influx calculations both in 2D and 3D was to tie in with previous calculations of flux steady-state, which were performed in 2D (Batt et al., 2001) and to test whether the assumed spatial geometry is important for the flux steady-state analysis. Indeed, the calculations both in 2D and 3D showed that different results are obtained, depending on the assumed geometry.

For the revised manuscript we will explain in more detail the reasons behind our sample selection for the inversion and why it matters, whether the flux analysis is performed in 2D or 3D.

We now explain in more details the reason behind our sample selection for the thermo-kinematic modelling in lines 246 – 252.

We reformulated the introduction, so that it now includes a short description of the approach of Batt et al. (2001) in lines 55 – 61 and emphasize that we want to explore whether steady state depends on the spatial geometry (lines 81 – 83). Because in our case we obtain steady-state only for a 3D geometry, we now highlight this in the discussion (lines 601 – 607) and conclusion (lines 721 – 725).

4) The organization of the paper itself could be better to help its readability (for instance there is no results section on steady-state itself, which is surprising having read the title of the paper).

In section 4.3 we provide results from our quantitative influx and outflux calculations but limit our explanations to only reporting the numbers. Any further elaboration (e.g. direct comparison between influx and outflux volumes) would already be discussion,

which can be found in section 5.4. This also pertains to the qualitative comparison between influx and outflux, based on variations on parameters like plate convergence rate, sediment thickness and exhumation rates.

5) The addition of this paper, compared to established literature (Batt et al., 2001; Brandon et al., 1998; Michel et al., 2018) that already demonstrated a global steady- state over the last 14 Myr and change of exhumation rate at the onset of the glaciations, is not clear to me.

With our approach of using multi-chronometer samples we are able to report a remarkably rich temporal exhumation history that represents a significant new contribution. Besides the increase at ~2–3 Ma (already reported by Michel et al. 2018) there is a decrease in exhumation rates occurring at ~6 Ma due to the decrease in plate convergence rate. Since the contribution of both tectonics and climate to the evolution of mountain belts is still a matter of active debate in the geoscience community, this result presented in the manuscript is of interest also to a broader readership.

In a previous study, Batt et al. (2001) concluded that the Olympic Mountains are in flux steady-state, because they successfully modeled their observed thermochronometer ages with a thermo-kinematic model (including horizontal velocities). However, a balance between influx and outflux is a basic precondition in deriving the mathematic equations for the model. Therefore, a flux steady-state balance is not directly tested, but deduced from their successful modeling. One might also argue that due to the non-uniqueness of modeling approaches (i.e. different models yield the same answer, depending on the considered parameter space), a direct corroboration of flux steady-state in the Olympic Mountains is still missing.

For our approach we tried to directly calculate both the influx and the outflux independently from each other, considering new constraints for parameters like sediment thickness, plate convergence rate and denudation rates. We also considered the temporal variations in these parameters, which has so far not been done. In addition to Brandon et al. (1998) and Batt et al. (2001) who focused their analyses on the long-term flux steady state over 14 Myr, we show that (at least qualitatively) strong temporal variations in influx and outflux occur on short timescales.

Hence, we believe that the results in this manuscript correspond to new results that complement the established literature and are of interest to a broad readership. As the reviewer also mentions in another comment below, we should more clearly explain how our methodology/approach differs from the established literature. We will do this in the introduction of the revised manuscript.

We significantly reformulated the introduction, so that it should now be more obvious what represents a new contribution. This includes indicating the hitherto unnoticed decrease in exhumation rates (lines 83 – 87), and pointing out how our approach for assessing flux steady-state is different from the approach of Batt et al. (2001). In the conclusion we emphasize that with our approach we only obtain flux steady-state for a three-dimensional geometry, contrary to the previous analysis (lines 723 – 725).

Detailed comments:

 # L 32-35: A very minor comment: steady-state is time-scale dependent, but it is also spatial-scale-dependent. The likelihood of obtaining a steady-state, for a given time-scale, is likely decreasing when going to finer spatial-scales due to heterogeneities and variabilities in landscape dynamics or tectonics that might become more and more dominant in controlling averaged or integrated values (i.e., mean topography or mountain range sediment discharge). This applies to topographic and flux steady-states. This dual dependency of steady state to time and spatial scales (if correct), implies that defining a steady-state over a time-scale can be a correct or incorrect assumption, depending on the associated spatial-scale. So please be clear and explicit on which spatial-scale you investigate here.

Thanks for this important remark. Indeed, as we showed with our flux steady-state analysis (performed both in 2D and 3D), the spatial geometry considered for the analysis is important. We will be clearer in the revised manuscript, which spatial geometries we investigate.

We reformulated this paragraph of the introduction, addressing now the spatial and timescale dependence of flux steady-state (lines 38 – 44).

 # L 51 - Please add a sentence to clearly state in the introduction, what are the main differences, in terms of methods and expected results, of this new manuscript compared to Michel et al. (2018) at Geology. Their abstract ends with: "However, the youngest AHe ages require a 50–150% increase in exhumation rates in the past 2–3 m.y. This increase in rates is contemporaneous with Pliocene-Pleistocene alpine glaciation of the orogen, indicating that tectonic rock uplift is perturbed by glacial erosion." Having read Michel et al. (2018), the differences are not clear to me at this stage of the paper (without having read the following sections).

Michel et al. (2018) focused on presenting results from thermochronometric dating (AHe and ZHe) and thermo-kinematic modeling, documenting the role played by the subduction zone geometry in driving rock uplift and the impact of Plio-Pleistocene

glaciation (increased exhumation rates due to glacial erosion). A direct test of flux steady-state was not the premise of that paper.

In the present contribution, we capitalize on multi-dating samples (additional AFT and ZFT ages), revealing an additional temporal variation in exhumation rates, which could not have been disclosed by Michel et al. (2018) due to the missing FT data. We also assess the flux steady-state balance by investigating both the influx and the outflux independently from each other.

To address the concerns of the reviewer we will convey more clearly in the revised manuscript what discerns the new contribution from previous work.

We reformulated the entire paragraph (lines 73 – 91), pointing out that the decrease in exhumation rate has not been discovered by Michel et al. (2018) and how our flux analysis is different from the approach of Batt et al. (2001).

 # L 202-207: I don't understand the need to use Pecube if neglecting topography and considering only a 1D model. An inverse modelling strategy using for instance QTQt (Gallagher et al., 2005 and so-on), that can jointly inverse samples from the same vertical profile, seems more appropriate here. This approach also has the benefit of not requiring any a priori time discretization. These advantages prevent the potential for both over interpretation and the introduction of artifacts in the inferred thermal histories.

It is important to emphasize that models such as HeFTy and QTQt are purely thermal models. These models are designed to be very good in calculating temperature-time paths based on thermochronometry information. However, for the purpose of this study we are exploring kinematic information (e.g., exhumation), and therefore, require a thermal-kinematic model such as Pecube. Furthermore, as we try to discuss in section 5.1 of the manuscript the information that can be obtained from our age-elevation transects is only limited due to the horizontal extent of the transects and the strong lateral gradient in exhumation rates within the Olympic Mountains. So, although vertical profiles can be directly included in QTQt, this might not yield ambiguous results.

Previous exhumation rates reported by Michel et al. (2018) for the Olympic Mountains were also derived by thermo-kinematic modeling using Pecube (however by using a 3D model). To tie in with previous work, we again used Pecube, but due to the suspected temporal variations in exhumation (as suggested by the thermochronometry data) we used the 1D model option coupled with a Monte-Carlo algorithm. This approach has

successfully been applied in other studies to derive exhumation rate histories, e.g. Ehlers & Thiede (2013), Adams et al. (2015), Avdievitch et al. (2018).

The issue mentioned by the reviewer regarding the timestep discretization is a good remark and requires more explanation. Our detailed response to that point can be found below and will be included in the revised manuscript.

 # L 230-236: What about isostasy or dynamic topography: are they not considered in the material influx? This need to be discussed.

We comment in detail on these points in our response below.

 # L 249-251: There might be some circularity in the rational (to assess steady-state), as sediment thickness depends on the outflux and controls the influx.

We thank the reviewer for pointing this out. This indeed is an aspect that represents a limitation to our approach. As we described in section 2.3 of the manuscript, the sediment currently entering the accretionary wedge is a mixture of sediment with different source regions (e.g. Olympic Mountains, Vancouver Island, Canadian Cordillera and in case of the Astoria fan the interior USA). Particularly with the onset of Plio-Pleistocene glaciation this effect became more pronounced, due to increased detrital input from the Cordilleran Ice Sheet. Hence, our influx/outflux calculations for the Olympic Mountains do not represent a closed system, where increased denudation in the Olympics (so a higher outflux) directly results in a higher influx (due to an increased sediment thickness).

However, our calculations indicate that on long timescales (i.e., the 14 Myr considered in the calculations) flux steady-state is reached, which might seem surprising given that the sediment thickness is governed by contributions from different source regions. We suspect that processes during sediment deposition, like redistribution by turbidity currents and re-deposition in more proximal parts of the Juan de Fuca plate, play an important role in the final sediment budget. In other words, the amount of sediment eroded from the Olympic Peninsula in a given time period (the outflux) is dispersed as it enters the ocean, so that for the same time period only a fraction of the sediment thickness (governing the influx) is composed of material originating from the Olympic Peninsula.

We now included a new section in the discussion (Section 5.5), where we discuss the limitations and restrictions of our approaches. The elaboration on this point mentioned by the refer can be found in lines 655 – 672.

 # L 295: "Our exhumation rates presented in this paper (Fig. 5) have a high temporal resolution". This statement might be overstated. No test was performed on the sensitivity of the inversion scheme and results to the time-step used (only 1 Myr was used). The data, especially individual samples, do not necessarily inform on a temporal evolution at a 1 Myr resolution. Is the inversion misfit better when changing temporal resolution? I would like to see some tests to determine the best time-step for the inversion (at least performed on one sample).

Our apologies, if our wording caused some misunderstanding. With this sentence we wanted to state that our 1D model is well suited to resolve temporal variations in exhumation rates, because the model covers a large range of possible exhumation histories. In comparison, the exhumation rates used in calculating the denudational outflux (the rates presented in Michel et al. 2018) have a good spatial coverage, but the 3D model is not suited to investigate a large range of possible exhumation histories. In the revised manuscript we will change the wording, so that our intension for using the exhumation rates during the flux calculations is more evident.

Nonetheless, the concerns of the reviewer regarding our chosen time-step interval are justified and need to be addressed. We will perform tests for a sample using different time steps. However, the time period resolved by our thermochronometer ages varies between 5 and 10 Myr for the seven considered samples, placing a threshold to possible durations of the time steps (e.g. durations longer than 3 Myr seem not to be reasonable). We also note, that although our reported exhumation rate histories in Figure 5 seem very detailed and suggest a high temporal resolution, these step-like patterns would likely be much smoother in reality. Hence our summary of exhumation rates in Figure 8 uses a more smoothed shape.

In the revised manuscript, we will present results from the sensitivity analysis of the time-steps.

We rephrased the statement the reviewer criticized so that it should now be less misleading (lines 380 – 383).

As requested, we also conducted additional simulations using different time step intervals and provide the results along with a brief discussion in the electronic supplement (in Section S2). We direct the reader to the supplement in lines 255 – 257 of the revised manuscript.

 # L 510 – section Results - Please add a sub-section at the end of the Results section, to present the results concerning flux steady-state analysis. This is the main ambition of this paper, and yet there is no result section on steady-state. This does not help the reader to get a clear message from reading this paper.

See our response to comment 4).

 # L 367 – section Discussion - Please add a sub-section to present the limitations of the approaches used in this paper.

A good suggestion by the reviewer. We will include a section in the revised paper, which addresses the aspects mentioned by referee #1 and #2 (e.g. limitations of our influx and outflux calculations, limitations of the exhumation rates).

As requested, we provide a new section (Section 5.5) discussing the limitations and restrictions of our approaches (lines 630 – 706).

 # L 385-390: For the vertical profile with ZHe data, the change of polarity of the slope is not a robust feature. Models can be defined, satisfying all the ZHe ages and their uncertainties, without leading to a change of slope. However, for AHe, the change of slope seems robust.

We agree with the reviewer that a line can also fit the ZHe ages (without a change in slope). In the revised manuscript, we will change this. Our further interpretation that the age elevation transects only yield limited information on exhumation rates should still be valid.

We changed Figure 4 in order to account for the comment made by the reviewer, and also reformulated the entire section about the age-elevation transects in the revised manuscript (lines 477 – 500).

 # L 451: It is assumed in this paper that the geometry of the accretionary wedge is constant and that other processes than tectonic accretion are negligible (an implicit assumption). Could you please discuss: 1) if there were some potential changes in the extent, volume and geometry of the Olympic Mountain accretionary wedge? 2) how you integrate isostasy or dynamic topography in your comparison of in- and out- fluxes? The isostatic response to

erosion can generate uplift (with no associated influx in the presented model) and induce additional erosion. This need to be discussed in this manuscript (not as a perspective L533-536).

We thank the reviewer for raising this issue and we will discuss it in more detail. For our quantitative assessment of flux steady-state we try to calculate the actual volumes of influx and outflux during the 14 Myr period. The two calculated fluxes should be viewed as pure volumes and separately from each other. Flux steady-state is attained, if both volumes (calculated for the 14 Myr period) equal themselves. We base our outflux calculations on the spatial integration of the exhumation rate pattern presented by Michel et al. (2018) and also consider the increase in exhumation due to the Plio-Pleistocene glaciation. As influx we consider all sediment resting on the subducting oceanic plate (so the influx is governed by the sediment thickness and the plate convergence rate). We assume that the mechanism of actual accretion (i.e., frontal accretion vs. sedimentary underplating) is not important, because finally all sediment is incorporated into the accretionary wedge and contributes to the influx volume, irrespective whether accretion takes place at the front of the accretionary wedge or at depth. As we discuss in the manuscript there are no estimates available on how much sediment might be transported into the mantle, so this is a limitation to our approach.

The impact of isostasy to the influx volume is not obvious to us. Any isostatic response (e.g. due to increased erosion during the Quaternary) affects the mountain range itself (so to say the volume of already accreted sediment material), but does not directly affect the influx volume. A possible increase in erosion related to isostatic uplift of course affects the outflux, as the reviewer noted (and in turn increases the influx, due to a higher sediment yield). If there was a significant change in rock uplift rates created by a change in isostatic compensation, then this would have likely changed exhumation rates, which would be recorded by our chronometers and seen in our modeling results. Therefore, there is no reason to directly account for isostatic compensation in our thermo-kinematic models.

Effects of the Plio-Pleistocene glaciation are already included in our calculations (see Table 5), like an increase in sediment thickness (affecting the influx) and an increase in denudation rates (affecting the outflux). So one could argue, that a possible contribution of the effects of isostatic uplift is already included in our calculations (but we can't quantify the exact contribution of isostasy). In total, the observable effects of Plio-Pleistocene glaciation are likely the combined effects of increased sediment supply (particularly by the Cordilleran Ice Sheet), and increased exhumation rates (due to glacial erosion).

The reviewer also asks, if there were some potential changes in the extent, volume and geometry of the accretionary wedge. These parameters are affected by the amount of accreted sediment and the dip of the subducted plate. As shown in Figure 1 the subducted plate displays a bend below the Olympic Mountains, resulting in a flatter angle of subduction compared to areas in the north or south. If bending the plate occurs through time (the reason for bending is hypothesized to be extension in the Basin and Range Province, Brandon & Calderwood 1990), then this indicates that the angle of subduction below the Olympic Mountains is likely variable through time and hence the volume and extent of the accretionary wedge is varying through time as well. Our reported cross sections (Figure 7) show that the volume and shape of the accretionary wedge is spatially variable. As stated in our manuscript, a change in the width and mechanics of the offshore part of the wedge has been observed due to increased sedimentation during the Quaternary (e.g. Adam et al., 2004). So, the temporal and spatial evolution of the accretionary wedge is complicated. However, our flux steady-state calculations should be independent from any changes in the shape of the accretionary wedge. As we outlined above, we only look at the calculated volumes of influx and outflux, which do not depend on any parameter affecting the shape of the accretionary wedge.

For the revised manuscript, we will include a discussion of the above points, likely in a section about the limitations of our approach, as also suggested by the reviewer.

As suggested by the reviewer, we included a new section (section 5.5) in the revised manuscript, where we discuss the points raised by the reviewer (lines 630 – 706).

 # L 505: "In summary, the assessment of flux steady state in the Olympic Mountains is non-trivial and many scenarios are possible." The used datasets (thermochronological data, sediment deposits, geometrical structure, etc) are not sufficiently well resolved to offer a robust assessment of temporal changes in fluxes or in steady-state. Therefore, one could question the real addition of this paper compared to Batt et al. (2001), Brandon et al. (1998) or Michel et al. (2018) that have already demonstrated 1) a global steady-state over the last 14 Myr and 2) a potential change in exhumation rate with the onset of Plio-Pleistocene glaciations.

In our response to the reviewer's comment 5) we already outlined what we view as new contributions. We fully understand that the reviewer is critical on this point. The Olympic Mountains have long been viewed as a case example for a (flux) steady-state mountain range. As we tried to convey in our manuscript our approach shows that both influx and outflux are subject to temporal variations (but as the reviewer notes, we can

not provide a full, quantitative assessment on small temporal scales). We believe that the results reported in this paper will stimulate further investigations of (flux) steady-state, so that in the future better and further constraints are available for parameters, which we could not include in detail (e.g. sediment data, margin parallel velocities). This could contribute to a new perspective and understanding of steady-state in active mountain ranges.

We reformulated parts of the discussion, so that section 5.4.2 now points out the difference between our approach and the approach of Batt et al. (2001), because we only observe flux steady-state for a three-dimensional geometry (lines 602 – 607). The rewritten conclusion is now also more specific about what new contributions were made with this manuscript (lines 707 – 733).

Minor edits:
 # L 14 : "We present 61 new thermochronometric ages" - Please add: mainly obtained from 21 new samples (or the correct number).

As requested, we will change this in the revised manuscript.

We added the correct number of new samples (line 15).

 # L 37: "tectonic parameters" – please change by "tectonic conditions" (a parameter implies a quantitative framework/model that has not been defined yet).

Good remark, will be changed in the revised manuscript.

We replaced the word "parameter" with condition at this location and also throughout the entire manuscript.

 # L 39: "Plio-Pleistocene glaciation" - There is probably no need to limit the scope to the onset of Plio-Pleistocene glaciation, as older glaciations (for instance at the Eocene- Oligocene transition; Bernard et al., 2016; Thomson et al., 2013) might have also led to variations in denudation and exhumation.

In the revised manuscript, we will no longer limit this to the Plio-Pleistocene glaciation and include references to earlier glaciations.

We include the two additional references mentioned by the reviewer, and no longer limit the effects of glaciation to the Plio-Pleistocene glaciation (lines 49 – 52).

 # L97: ref "Ehlers et al. 2005" : The closure temperature of these thermochonometers has been constrained in older papers than Ehlers, 2005. For instance: Gallagher et al., 1998; Farley, 2002; ...

Additional references will be included in the revised manuscript.

We included an appropriate reference for each thermochronometer system (line 133).

 # L 162: "three/two" - What does three/two mean here?

This indicates the number of samples collected for this study, which have been dated with AFT and ZFT, respectively. We will reword this in the revised manuscript.

The reworded phrase, which is now more explicit, can be found in lines 221 – 222.

Marked-up version of revised manuscript:

How steady are steady-state mountain belts? – a re-examination of the Olympic Mountains (Washington State, USA)

Lorenz Michel[1], Christoph Glotzbach[1], Sarah Falkowski[1], Byron A. Adams[1,2], Todd A. Ehlers[1]

[1]Department of Geosciences, University of Tübingen, Tübingen, 72074, Germany
[2]School of Earth Sciences, University of Bristol, Bristol, BS8 1RJ, United Kingdom

Correspondence to: Todd A. Ehlers (todd.ehlers@uni-tuebingen.de)

Abstract. The Olympic Mountains of Washington State (USA) represent the aerially exposed accretionary wedge of the Cascadia Subduction Zone and are thought to be in flux steady-state, whereby the mass outflux (denudation) and influx (tectonic accretion) into the mountain range are balanced. We use a multi-method approach to investigate how temporal variations in the influx and outflux could affect previous interpretations of flux steady-state. This includes analysis of published and new thermochronometric ages for (U-Th)/He dating of

apatite and zircon (AHe and ZHe, respectively) and fission track dating of apatite and zircon (AFT and ZFT, respectively), 1D thermo-kinematic modelling of thermochronometric data, and independent estimates of outflux and influx.

In total, we present 61 new AHe, ZHe, AFT, and ZFT thermochronometric ages from 21 new samples. AHe ages are generally young (<4 Ma), and, in some samples, AFT ages (5–8 Ma) overlap with ZHe ages (7–9 Ma) within uncertainties. Thermo-kinematic modelling shows that exhumation rates are temporally variable, with rates decreasing from >2 km/Myr to <0.3 km/Myr around 5–7 Ma. With the onset of Plio-Pleistocene glaciation, exhumation rates increased to values >1 km/Myr. This demonstrates that the material outflux is varying through time, requiring a commensurate variation in influx to maintain flux steady-state. Evaluation of the offshore and onshore sediment record shows that the material influx is also variable through time and that the amount of accreted sediment in the wedge is spatially variable. This qualitatively suggests that significant perturbations of steady-state occur on shorter timescales (10^5–10^6 yr), like those created by Plio-Pleistocene glaciation. Our quantitative assessment of influx and outflux indicates that the Olympic Mountains could be in flux steady-state on long timescales (10^7 yr), but that flux steady-state also depends on the assumed spatial geometry.

1 Introduction

The assumption of a balance between opposing processes has allowed geoscientists to use proxy measurements (like denudation rates) to constrain difficult to measure variables like rock uplift. This has given rise to the concept of steady-state landscapes or mountain ranges. Likewise, a steady-state (i.e., a mass balance) is commonly one of the boundary conditions in modelling studies investigating the evolution and dynamics of orogens in response to changes of other boundary conditions like climate or tectonic fluctuations (e.g., Batt et al., 2001; Stolar et al., 2007; Whipple and Meade, 2006; Willett, 1999). Two main types of steady-state are often

used to interpret mountain building processes (e.g., Willett and Brandon, 2002): (1) Topographic steady-state, where the topography is invariant, because rock uplift and horizontal motion of material is balanced by denudation, and (2) flux steady-state, where the material influx (by accretion of sediment and rock) is balanced by the material outflux (by denudation) from a mountain range. The assumption of steadiness is both spatial- and timescale-dependent so that for a given timescale, steadiness might only be achieved on a large, orogen-wide spatial scale, due to the spatial averaging of single processes acting on a small scale (e.g., catchment-wide sediment discharge vs. orogen-wide sediment discharge). Furthermore, a possible perturbation of steady-state is sensitive to the timescale it takes for orogens to respond to variations in crustal deformation or a change in climate. If the timescales required for a change in the influx and outflux are significantly different from each other, a deviation from steady-state is likely.

Likewise, studies from different orogens worldwide suggest strong variations in denudation and exhumation on million-year timescales. These variations can be linked to changes in the tectonic conditions (e.g., Adams et al., 2015; Lease et al., 2016), internal dynamics of drainage basins (e.g., Willett et al., 2014; Yanites et al., 2013), changes in the magnitude of precipitation (e.g., Lease and Ehlers, 2013; Whipple, 2009), or the onset of glaciation (e.g., Berger et al., 2008; Bernard et al., 2016; Ehlers et al., 2006; Glotzbach et al., 2013; Gulick et al., 2015; Herman et al., 2013; Herman and Brandon, 2015; Lease et al., 2016; Thomson et al., 2010; Thomson et al., 2013; Valla et al., 2011; Yanites and Ehlers, 2012).

Based on thermo-kinematic modelling of thermochronometric cooling ages, the Olympic Mountains, USA, (Fig. 1a) have been proposed to be in flux steady-state since ca. 14 Ma (Batt et al., 2001; Brandon et al., 1998). The approach of these studies was to assume flux steady-state along a two-dimensional profile across the Olympic Peninsula as a precondition in order to derive the kinematics of the model from the balance between accretionary influx (governed by the thickness of accreted sediment and plate convergence rate) and denudational

outflux (as set by exhumation rates). Because the cooling ages can successfully be modelled with the used kinematics, the mountain range is then interpreted to be in flux steady-state. However, possible temporal variations in parameters like sediment thickness, plate convergence rate or exhumation rates were not considered in these studies. Likewise, the impact of Plio-Pleistocene glaciation on the flux steady-state hypothesis has not been considered yet, although the range was extensively incised by glaciers (Adams and Ehlers, 2017; Montgomery, 2002; Montgomery and Greenberg, 2000; Porter, 1964) and experienced significant changes in climate conditions over the past 3 Myr (Mutz et al., 2018). Numerical modelling studies investigated the mechanics of the wedge by either considering fluvial erosion (Stolar et al., 2007) or glacial erosion (Tomkin and Roe, 2007). A significant response of the orogenic wedge to glaciation was suggested (Tomkin and Roe, 2007) and recent studies proposed that exhumation rates in the Olympic Mountains increased due to Plio-Pleistocene glacial erosion (Herman et al., 2013; Michel et al., 2018). Resulting high sedimentation rates during the Quaternary increased the sediment thickness on the oceanic plate and seem to have caused a change in the deformational style of the offshore part of the wedge (Adam et al., 2004).

In this study, we test the hypothesis of flux steady-state in the Olympic Mountains, considering variations in both the material influx and outflux. First, we test the temporal steadiness of exhumation rates from bedrock cooling histories with a 1D thermo-kinematic model, capitalizing on new samples which have been dated with three to four thermochronometers (apatite and zircon (U-Th)/He and fission-track data; AHe, ZHe, AFT, and ZFT, respectively). Second, instead of assuming flux steady-state as a precondition, we attempt to estimate both the accretionary influx and denudational outflux independently from each other. We particularly consider possible temporal variations in parameters affecting both fluxes by using published data of the off- and onshore sediment records, and exhumation rates from thermochronometry. To tie in with the previous flux steady-state assessment in the Olympic Mountains (which was performed in two dimensions), we evaluate whether the spatial geometry (two- or three-dimensional) used for the flux calculations is important. With our new

thermochronometry data we reveal a previously undetected temporal variation in exhumation rates due to a change in the tectonics (a reduction in plate convergence rates that resulted in a decrease in exhumation rate), as well as the previously reported increase in exhumation rates related to the Plio-Pleistocene glaciation (reflecting a change in climate). Similarly, both material influx and outflux are temporally variable, especially during the Quaternary. A quantitative comparison between both fluxes suggests that the Olympic Mountains could be in flux steady-state, but only over longer timescales (e.g., 10^7 yr), and also demonstrates that it is essential to consider the spatial geometry used for a flux steady-state assessment (i.e., two- vs. three-dimensional).

2 Background

2.1 Geology and glacial history of the Olympic Mountains

At present, the Juan de Fuca Plate subducts obliquely with respect to the overriding North American Plate (Fig. 1a) at 34 mm/yr at the latitude of the Olympic Mountains (Doubrovine and Tarduno, 2008). The forearc high of the subduction zone comprises (from north to south) Vancouver Island, the Olympic Mountains and the Oregon Coast Range, and lies west of a forearc low (e.g., Georgia Lowlands, Puget Lowlands) and the active volcanic arc (Fig. 1a). Seismic imaging suggests a flatter subduction angle beneath southern Vancouver Island and the Olympic Mountains (Hayes et al., 2012; McCrory et al., 2012), compared to areas in the north and south (Fig. 1a). The modern configuration of the subduction zone was established by the latest Eocene (e.g., Brandon and Vance, 1992) after accretion of the Coast Range Terrane to the North American continent (Fig. 1c). This terrane represents a large oceanic plateau and extends from the southern tip of Vancouver Island to Oregon (Eddy et al., 2017; Phillips et al., 2017; Wells et al., 2014).

The accretionary wedge of the subduction zone is exposed onshore within the Olympic Mountains (Fig. 1a) and is composed of Eocene–Miocene flysch (Brandon et al., 1998; Tabor and Cady, 1978). This part of the

mountain range is known as the Olympic Structural Complex (Brandon et al., 1998) and is separated from the surrounding Coast Range Terrane by the Hurricane Ridge thrust fault (HRF; Fig. 1c), a major discontinuity traceable in seismic surveys (e.g., Clowes et al., 1987; Calvert et al., 2011). Minor sedimentary rocks of Eocene age (Eddy et al., 2017; Tabor and Cady, 1978) are contained within the Coast Range Terrane besides the predominant ~50 Ma old marine and subaerial basaltic rocks (Eddy et al., 2017). Exhumation of the range commenced at 18 Ma and since 14 Ma, the orogen is supposed to be in flux steady-state (Batt et al., 2001; Brandon et al., 1998; Pazzaglia and Brandon, 2001).

Plio-Pleistocene glaciation has strongly influenced the present-day appearance of the Olympic Mountains (Fig. 1b). During its maximum extent at ~14 ka, the Cordilleran Ice Sheet advanced from the Coast Mountains of British Columbia and covered Vancouver Island and large parts of todays' continental shelf (Booth et al., 2003; Clague and James, 2002). The Puget and Juan de Fuca lobes of the Cordilleran Ice Sheet surrounded the Olympic Mountains in the east/southeast and in the north, respectively (Fig. 1b). Alpine glaciers incised deep valleys in the landscape, particularly on the western side of the range (Adams and Ehlers, 2017; Montgomery, 2002), where piedmont glaciers almost reached the Pacific Ocean (Thackray, 2001). Glacial erosion varied across the range, as the location of the Pleistocene equilibrium line altitude increases from 1000 m in the west to 1800 m in the east (Porter, 1964), due to a strong precipitation gradient (> 6000 mm/yr in the west, < 1000 mm/yr in the east). Determining the exact onset of glaciation in the Olympics has proven difficult, but the oldest deposits of the Cordilleran Ice Sheet in the Puget Lowland are as old as 2 Ma and deeply weathered alpine till on the west side of the Olympics is interpreted to be of the same age (Easterbrook, 1986).

2.2 Previous thermochronometry studies in the Olympic Mountains

Within the Olympic Mountains, an extensive dataset of thermochronometric cooling ages from bedrock samples (Figs. 1b and 2) exists for AHe (Batt et al., 2001; Michel et al., 2018), AFT (Brandon et al., 1998), ZHe

(Michel et al., 2018) and ZFT (Brandon and Vance, 1992; Stewart and Brandon, 2004). These thermochronometer systems record cooling through a temperature range of ~60–240°C (e.g., Brandon et al., 1998; Farley, 2002; Gallagher et al., 1998; Reiners et al., 2004), as they have effective closure temperatures of 70°C, ~120°C, ~180°C and ~240°C, respectively, for a cooling rate of ~10°C/Myr (Ehlers, 2005). The interpretation of thermochronometric cooling ages from sedimentary rocks (such as in the Olympic Mountains) is often complicated when the cooling signal from the sediment source region(s) has not been reset due to reheating during subduction and metamorphism. If a sedimentary rock sample has not had sufficient exposure to temperatures above the closure temperature of a given thermochronometer, the sample might retain cooling ages that represent the source region's cooling history (referred to as unreset) or might be a mixture of provenance cooling histories and the reheating process (incompletely reset sample). Determining, whether a sample is completely, incompletely or un-reset can be difficult and usually depends on the statistics of cooling age populations, derived from the dated mineral grains (e.g., Brandon et al., 1998). The reproducibility of single grain (U-Th)/He ages from a sample provides an indication of whether a sample is reset or not. This is typically determined with n=4–7 grains. For the fission track method, a larger number of grains is typically dated (n=20–100) to reduce the uncertainty in the final cooling age calculation. For samples with a large population, statistical methods can be applied to decompose the chronometer date distribution into different populations, and to determine if some portion of the sample is reset (Brandon, 1992, 1996). In the case where a sample is incompletely reset, a significant young age peak is determined and interpreted as the sample cooling age (e.g., Brandon et al., 1998).

In the Olympics, the youngest published reset AHe ages (≤ 2.5 Ma) can be found in the western and central portions of the mountain range, and there are two unreset samples in the east (Fig. 2a). The pattern of AFT ages is more complicated (Fig. 2b), and most reset and incompletely reset samples are located in the central part of the mountain range, whereas unreset samples are restricted to areas outside the central (high topography) part of the

range. The youngest reported AFT samples (2–4 Ma) are incompletely reset samples and fully reset samples have cooling ages between 7 Ma and 27 Ma. ZHe data show a well-developed trend of unreset cooling ages at the coast and reset 5–6 Ma ages in the headwaters of Hoh and Elwha rivers (cf., Figs. 1b and 2c). Reset ZFT samples (~13–14 Ma) are confined to a small area east of Mt. Olympus (Fig. 2d).

Based on thermo-kinematic modelling, Michel et al. (2018) attributed the observed AHe and ZHe age pattern to an ellipse-shaped exhumation pattern (with highest exhumation rates in the central, high-topography part of the mountain range, Fig. 2e), as predicted for a mountain range situated in an orogenic syntaxis setting (Bendick and Ehlers, 2014). Here, a bend in the subducted slab creates a mechanical stiffening, which in turn leads to rapid and focused exhumation at the surface (Bendick and Ehlers, 2014). High uplift rates in the central, high topography part of the mountain range are also corroborated by topographic analyses (Adams and Ehlers, 2017) and denudation rates based on cosmogenic nuclides (Adams and Ehlers, 2018). Furthermore, modelling of particularly young AHe ages (<2.5 Ma) suggests that exhumation rates increased significantly by 50–150 % due to Plio-Pleistocene glacial erosion (Michel et al., 2018).

2.3 Offshore sediment record

Data constraining the sediment thickness on the Juan de Fuca Plate before incorporation of sediment into the accretionary wedge are summarized in Figure 3. Three boreholes were drilled into the blanketing sediments of the Juan de Fuca Plate during deep-sea drilling projects (ODP 888, ODP 1027 and DSDP 174; Fig. 3 and Table 1), and provide estimates of the sediment thickness and age constraints. The sediment thickness at the deformation front of the subduction zone has been estimated from three seismic studies (Adam et al., 2004; Booth-Rea et al., 2008; Han et al., 2016).

Most of the sediment is contained within two deep-sea sediment fans with different sediment sources. Today, sediment sources for the Nitinat Fan (offshore Vancouver Island and the Olympic Mountains) include detritus from Vancouver Island, the Olympic Mountains, and material delivered by the Fraser river system (Fig. 3), which drains large parts of the Canadian Cordillera including the British Columbian Coast Mountains (Carpentier et al., 2014; Kiyokawa and Yokoyama, 2009). The Astoria Fan offshore the Oregon coast is mostly fed by the Columbia River and is sourced by a large area in the interior of the USA (Fig. 3).

The total sediment thickness varies between 2600–3500 m at the deformation front and decreases rapidly to 600 or 900 m approximately 100 km away from the deformation front. At the locations of ODP 1027 and DSDP 174, up to 50–70 % of the total sediment thickness are Quaternary deposits, and sedimentation rates more than doubled during the Quaternary (from 80–110 m/Myr to 250–270 m/Myr, Table 1). At the location of ODP 888 the drilled 570 m of core were deposited over the past 600 kyr, suggesting very high sedimentation rates of 950 m/Myr compared to 400 m/Myr for the total sediment thickness of 2600 m at the location of the core (Table 1). As determined from detailed, stratigraphic analysis of core ODP 888, sedimentation rates are also highly variable during the Quaternary. Rates during glacial periods can be as high as 1900 m/Myr compared to 700 m/Myr during interglacials (Knudson and Hendy, 2009). At sites ODP 888 and 1027, the source region of the sediments has been the Canadian Cordillera for the past 3.5 Myr, which has not been affected by glacial-interglacial cycles (Carpentier et al., 2014; Kiyokawa and Yokoyama, 2009). The provenance of the sediments at DSDP 174 is mostly the Proterozoic Belt Supergroup in the interior of the USA and differs significantly from present-day detritus of the Columbia River (Prytulak et al., 2006). Hence, Prytulak et al. (2006) suggest that deposition of the upper 630 m of sediment at this site and the build-up of the Astoria Fan were governed by glacial outburst floods.

3 Methods

We use a multi-method approach to assess flux steady-state in the Olympic Mountains. This includes thermochronometric dating, thermo-kinematic modelling of cooling ages to obtain exhumation rates, and independent estimates of accretionary influx and denudational outflux. We calculate the influx based on constraints of the incoming sediment thickness and plate convergence rate, and the outflux based on spatial constraints of exhumation rates within the Olympic Mountains. The procedure for each method is outlined below.

3.1 Thermochronometric methods

Our strategy with thermochronometric dating was (1) to obtain samples, which are multi-dated with up to four thermochronometer systems (because these are particularly sensitive to reveal variations in exhumation rate) and (2) to collect samples within vertical profiles in order to obtain estimates of the exhumation rate at the site of the respective profile. Therefore, we dated several literature samples with additional thermochronometer systems (Table 2) and we also present 19 new bedrock samples from vertical profiles (Fig. 4, Table 2) and two additional bedrock samples (OP1528 and OP1556; Fig. 2, Table 2) collected at an elevation of ~400 m, enlarging the existing ~400 m equal-elevation data of Michel et al. (2018). All new samples are sandstones of varying grain size. A sample transect at Mt. Olympus extends from the bottom of the Hoh Valley to the apex of the Olympic Peninsula (Mt. Olympus, 2428 m), covering ~2 km of relief (Figs. 4a and b). The Mt. Anderson transect starts in the upper reaches of the Quinault Valley and terminates on the flank of Mt. Anderson covering a total elevation difference of ~1600 m (Figs. 4a and c). The Blue Mountain transect is located in the northern part of the Olympic Peninsula close to Blue Mountain, covering an elevation difference of ~1300 m (Figs. 4a and d). All collected samples were dated with the AHe and ZHe techniques, three of these were dated by AFT, and two were dated by the ZFT technique. Additionally, we dated 13 samples from Michel et al. (2018) by AFT and five by ZFT thermochronometry. This process yielded seven samples with AHe, AFT, ZHe and ZFT cooling ages (Table 2).

Standard mineral separation techniques (sieving, magnetic and gravimetric separation) were used to obtain apatite and zircon separates from crushed rock samples. For AHe and ZHe dating mineral grains were hand-picked and dated in the thermochronometry lab of the University of Tübingen, following the dating protocol of Stübner et al. (2016). The Ft-correction for apatite (Farley, 2002) and zircon (Hourigan et al., 2005) is applied to the measured amount of helium. The (U-Th)/He age equation is solved using the approach of Meesters and Dunai (2005). From each sample, we dated 4–7 apatite grains or 3–6 zircon grains and the results of single-grain analyses can be found in Tables S1 and S2. Our approach for assessing whether a sample is reset or unreset and the procedure for exclusion of outliers is explained in the supplementary material (Section S1.1). For reset samples, we calculate the arithmetic mean age from the accepted single-grain ages, which is reported in Table 2 along with a one standard deviation (1SD) uncertainty.

Fission-track dating of apatite and zircon was performed using the external detector and the ζ-calibration techniques (Hurford, 1990). Details about the treatment of the apatite and zircon mounts in the Tübingen thermochronometry laboratory can be found in Falkowski et al. (2014) and Falkowski and Enkelmann (2016). Table 3 contains the AFT and ZFT sample ages, and explains the procedure for assessing whether a sample is reset or unreset. Data for single-grain ages from fission-track dating of apatite and zircon are reported in Tables S3 and S4.

3.2 Thermo-kinematic modelling: model setup and boundary conditions

To interpret cooling histories recorded by our thermochronometers as exhumation histories, we used a modified version of the thermo-kinematic model Pecube (Braun, 2003), which contains a built-in Monte Carlo approach to resolve temporal variations in exhumation histories (Adams et al., 2015; Thiede and Ehlers, 2013). The model allows exploring possible exhumation histories for a particular sample by varying exhumation rates through time at defined time steps. The accuracy of a particular exhumation rate history is estimated by

comparing modelled with observed cooling ages. More age constraints, and hence thermochronometer systems, lead to better resolved, modelled exhumation histories. Therefore, although we report 21 new thermochronometric ages, we only used the seven samples, which have age constraints from AHe, AFT, ZHe, and ZFT in our modelling efforts (OP1513, OP1517, OP1533, OP1539, OP1551, OP1573, OP1582; Table 2).

Thermo-physical parameters chosen for the modelling are typical values reported for the sandstones of the Olympic Mountains (Table 4). We initiated the models at 20 Ma and used a time step interval of 1 Myr with a maximum testable exhumation rate of 6 km/Myr. While our results are not sensitive to a 1 Myr time step, an assessment of time step intervals different from 1 Myr can be found in the supplementary material (Section S2). For each sample, we ran 20,000 simulations (each corresponding to a different exhumation history) and assessed the goodness of fit between observed and modelled data for the respective exhumation history, using a reduced χ^2-test. Here, sample ages τ_o were compared with modelled ages τ_m, using the uncertainty of the sample age σ_o for the number (N) of thermochronometer systems available for the respective sample:

$$\chi^2 = \left(\left(\frac{(\tau_o-\tau_m)^2}{\sigma_o^2}\right)_{AHe} + \left(\frac{(\tau_o-\tau_m)^2}{\sigma_o^2}\right)_{AFT} + \left(\frac{(\tau_o-\tau_m)^2}{\sigma_o^2}\right)_{ZHe} + \left(\frac{(\tau_o-\tau_m)^2}{\sigma_o^2}\right)_{ZFT}\right) \cdot \frac{1}{N} \quad (1)$$

If $\chi^2 \leq 2$, a specific model run was accepted as good. The number of accepted exhumation histories is shown in Figure 5 for each sample. From the range of acceptable exhumation rates at each time step (shown as blue shaded areas in Fig. 5), we calculated the mean exhumation rate together with 1 standard deviation for each time step (red/dashed lines and grey areas in Fig. 5). Although the model provides output for the entire model duration of 20 Myr, a meaningful exhumation rate can only be obtained for the time interval between oldest thermochronometric age of a sample and today (shown in Fig. 5).

For our purpose, we focus on exploring temporal variations in exhumation rates and therefore use a 1D model, where each sample is modelled independently from each other. In a 1D model, heat transport and

movement of particles is only considered in the vertical dimension within a column of rock, ignoring topography. This mode of modelling was selected because it allowed us to efficiently perform thousands of simulations quickly in order to cover a large range of possible exhumation rates. The high number of exhumation histories accurately predicts our observed cooling ages and allows for a robust statistical assessment of the best-fitting exhumation history. Previous publications addressing exhumation histories in other orogens have also highlighted that 1D models are often sufficient to explain most of the signal recorded in thermochronometric systems (e.g., Adams et al., 2015; Thiede and Ehlers, 2013). In the Olympic Mountains, Michel et al. (2018) argued that exhumation histories for the thermochronometer systems considered here can be well explained by vertical velocity paths, too. Because the spatial resolution of our seven considered samples is poor and they are all from the interior part of the mountain range (Fig. 4), we cannot further resolve the exhumation rates outside this area, making a 3D model very difficult to validate. Therefore, we limit our interpretations to the better-resolved exhumation histories from the 1D model and focus on the primary temporal changes, rather than paleotopography, or specific differences in the exhumation rates between samples.

Five of the seven considered samples are from the same elevation range (400–580 m), but two samples are from higher elevations (1360 m and 1500 m, Fig. 5). Large differences in elevation between the samples can impact the direct comparison between them (e.g., it can affect how changes in exhumation rate are recorded from location to location). However, we are not able to correct for this circumstance (by using an age elevation relationship), and therefore try to consider this complication when interpreting our exhumation rate histories from the different samples.

3.3 Methods for estimating flux steady-state

To assess the flux steady-state hypothesis of the Olympic Mountains, we need independent estimates of the material influx and outflux over time. For this, we focus on the time period since 14 Ma, which corresponds

to the proposed establishment of flux steady-state (Batt et al., 2001; Brandon et al., 1998). Flux steady-state requires that the material influx into the wedge equates the amount of accreted material, removed from the subducting slab. We assessed the amount of accreted sediment (material influx) with two approaches. First, we calculated the amount of sediment incorporated into the accretionary wedge at the deformation front (Fig. 6a) during the 14 Myr period. Second, we compared this amount of "expected" accreted sediment with the observed amount of sediment residing in the accretionary wedge along two cross sections. The material outflux from the mountain range is estimated using results from thermo-kinematic modelling, by equating modelled exhumation with denudation, which can then be integrated spatially and over the 14 Myr period.

The previous flux steady-state analyses in the Olympic Mountains were performed in two dimensions along a profile crossing the Olympic Peninsula. However, exhumation rates within the Olympic Mountains are known to vary spatially (Brandon et al. 1998; Michel et al., 2018). This suggests that the outflux is spatially variable, depending on the location within the mountain range. To tie in with the previous flux analyses we performed our analysis also in two dimensions, but additionally investigated a three-dimensional geometry to account for the spatially variable exhumation rates. The resulting geometries for the influx and outflux are summarized in Figure 6.

3.3.1 Calculating the accretionary influx

We used a similar approach as Batt et al. (2001) to calculate the accretionary influx, but we also considered temporal variations of the used variables. Assuming all sediments resting on the subducting oceanic crust are incorporated into the accretionary wedge, the volume of accreted sediment (V_{sed}) can be approximated using the porosity of the sediment η, incoming sediment thickness d, the duration of subduction t, and the subduction velocity perpendicular to the present-day deformation front u_{per}:

$$V_{sed} = \eta \cdot d \cdot t \cdot u_{per} \quad (2)$$

A limitation to this approach is the assumption that all sediment resting on the down-going plate is accreted. There is geochemical evidence that, at early stages of subduction at the Cascadia Subduction Zone, sediment has been incorporated into the mantle and been involved in the magmatism of the Cascades Arc (Leeman et al., 2005; Mullen et al., 2017). However, there are no estimates on the amount of sediment transported into the mantle at present, and most sediments seem to be accreted, either at the deformation front or underplated at depth (Calvert et al., 2011).

The variable with the greatest uncertainty in this calculation is the sediment thickness. As discussed above (Section 2.3), the present-day sediment thickness of 2.5 km is the product of increased offshore sedimentation during the Quaternary and the pre-Quaternary sediment thickness is difficult to determine. Following the approach described in the supplementary material (Section S3.1), we estimated a pre-Quaternary sediment thickness of 1.5 km. In total, we calculated three different sediment volumes based on different sediment thicknesses (Table 5). Assuming a thickness of 1.5 km and 2.5 km for the 14 Myr period yields a minimum and maximum value for the accreted sediment volume, respectively, representing a sediment volume unaffected by Quaternary sedimentation (1.5 km) and a volume for a likely too high sediment thickness, using the modern thickness (2.5 km). Alternatively, we considered an increase in sediment thickness from 1.5 km to 2.5 km at 2 Ma, which likely yields the geologically most meaningful volume.

The porosity of the sediment stack depends on the thickness and decreases with increasing overburden. According to Yuan et al. (1994), the porosity at depth z of the sediment stack can be approximated by

$$\eta = 0.6 \cdot e^{-z} \quad (3)$$

960 Using this equation, we calculated mean porosities of 31% and 22% for our sediment thicknesses of 1.5 km and 2.5 km, respectively.

Because the dip direction of the present-day deformation front is 72° (Φ_{def}) and we only considered accretion perpendicular to the deformation front, we corrected the convergence rate (u) by using the convergence angle (Φ) between the Juan de Fuca and the North American plates:

965 $$u_{per} = u \cdot \frac{\sin(\phi)}{\sin(\phi_{def})} \quad (4)$$

Both convergence rate and angle are variable over time and, therefore, we capitalized on the plate reconstruction model of Doubrovine and Tarduno (2008) to estimate these parameters over the past 14 Myr. Values shown in Figures 6b and 6c were calculated using the East-West Antarctica plate circuit model from Doubrovine and Tarduno (2008) for two different rotation models (Farallon M1 and M2 in the original
970 publication). This yields a range of possible convergence rates and angles, providing an uncertainty on the calculated sediment volume. The temporal resolution is given by the number of magnetic isochrons used for the plate circuit reconstruction by Doubrovine and Tarduno (2008).

From the temporal evolution of the corrected convergence rate (Fig. 6b), we calculated the sediment volume V_{sed} accreted during the 14 Myr period using Equation 2 and the parameters discussed above. We report
975 sediment volumes for two-dimensional and three-dimensional accretionary influx (Table 5). For the two-dimensional scenario, sediment can be viewed as being accreted at a single vertical column at the deformation front (Fig. 6a). For the three-dimensional scenario, accretion occurs along a vertical plane at the deformation front (Fig. 6a), and results obtained from Equation 2 are multiplied by a length (l). The coastline and the deformation front are approximately parallel to each other at the latitude of the Olympic Mountains. Hence, the

length of the coastline in the area is used for integrating the exhumation rates to the required length of the deformation front. This yields a value of 131 km for the length (see Fig. 6d).

3.3.2 Sediment volumes along cross-sections

We estimated the actual volume of sediment currently residing in the accretionary wedge along two cross-sections, which are approximately 50 km apart (Profile 1 and 2 in Fig. 7). The lower boundary of the accretionary wedge is the top of the subducting oceanic plate, which is constrained from the Slab 1.0 model (Hayes et al., 2012; McCrory et al., 2012). The upper boundary is defined by the present-day topography/bathymetry (from 10 m- and 500 m-resolution digital elevation models, respectively) and the Hurricane Ridge Fault (HRF). At the surface, the location of the HRF is adopted from a geologic map (Tabor and Cady, 1978) and below the surface we use information provided by a seismic study at depths of 22 km and 34 km (Calvert et al., 2011). The uncertainty related to the position of the HRF (error bars at HRF nodes in Fig. 7) was propagated to estimate an uncertainty for the calculated sediment volumes. Further explanation of this approach is given in the supplementary material (Section S3.2). Because the location of the HRF is not resolved at greater depths, we truncate the area considered for volume calculation at 34-km depth. Finally, the calculated volume is corrected for the porosity of the sediment stack, assuming an average porosity of 6%, similar to Davis and Hyndman (1989).

3.3.3 Calculating the denudational outflux

In the absence of extensional faults, denudation acts as the prime mechanism for exhumation in the Olympic Mountains. Therefore, exhumation can be equated with denudation and the denudational outflux from the range can be obtained from the spatial and temporal integration of exhumation rates.

The exhumation histories presented in this paper (Fig. 5) are well-suited to resolve temporal variations in exhumation, and hence provide qualitative information about variations in the denudational outflux. The low spatial density of the seven considered samples prohibits a quantitative assessment of the denudational outflux. To overcome this problem, we reverted to the pattern and exhumation rates suggested by Michel et al. (2018), providing good spatial coverage of almost the entire Olympic Peninsula (Fig. 6d). The total amount of exhumation, which is used for calculating the outflux and corresponds to the temporal integration of the exhumation rates, is similar within uncertainty in both data sets. For example, the modelled exhumation rate is sufficient to explain the ZHe age of 10.2 Ma for sample OP1513 in both studies (Michel et al., 2018 and this study).

Using the pattern and rates displayed in Figure 6d, we considered the outflux for two- and three-dimensional geometries to compare the calculated volumes with the values derived from the two- and three-dimensional influx calculations. In the two-dimensional scenario, we extracted the exhumation rates along a line, crossing the Olympic Peninsula (Fig. 6d) and the values for the integrals along this line are shown in Figure 6e. In the three-dimensional scenario, we spatially integrated over the entire pattern of exhumation rates (Fig. 6d). In both scenarios, we temporally integrated over the 14 Myr period. Additional to a constant exhumation scenario, we also considered an increase in exhumation rates, which is related to an increase in erosion due to Plio-Pleistocene glaciation of the Olympic Mountains (Michel et al., 2018). In Table 5, we report denuded volumes for the case of constant exhumation rates, and for the two possible increase scenarios suggested by Michel et al. (2018), equating a 50% increase in rates occurring at 3 Ma or a 150% increase in rates occurring at 2 Ma.

4 Results

4.1 Thermochronometry

Along the Mt. Olympus elevation transect (Fig. 4b), AHe ages (1.9–3.7 Ma) overlap with each other within sample error (except for the uppermost sample). ZHe ages (4.8–8.5 Ma) show a similar behaviour (with the exception of the lowermost sample; Fig. 4b). AFT ages for two samples are 5.1 Ma and 6.2 Ma, and the obtained ZFT ages of this transect are all unreset. Within the Mt. Anderson transect (Fig. 4c), AHe ages (1.5–3.9 Ma) increase with elevation up to an elevation of 1400 m and decrease between 1400 and 2100 m. ZHe ages vary between 6.5–8.9 Ma and one sample at ~1400 m has an AFT age of 7.8 Ma. For the Blue Mountain transect (Fig. 4d), AHe ages (3.6–30.1 Ma, and one unreset sample) do not show a clear correlation with elevation, but, interestingly, the uppermost sample yields the youngest age. ZHe ages of dated samples of this transect are all unreset.

Clear spatial patterns for the multi-dated thermochronometer samples are observable (cf., Fig. 2 and 4). AHe ages are reset (apart from one sample in the north-east of the mountain range) and decrease towards the centre of the mountain range, where very young ages (< 2.5 Ma) can be found. Seven fully reset AFT samples (5.0–7.8 Ma) are confined to the centre of the range (samples OP1513, OP1517, OP1533, OP1539, OP1551, OP1573, OP1582), overlapping with the area of reset ZHe samples. The remaining eight AFT samples are unreset (Table 3 and Fig. 4). Two samples at the north and east coast (OP1502 and OP1510) have the youngest age peaks at 26 Ma (comprising 29% of the dates) and 36 Ma (35%), respectively. Samples from the western part of the mountain range (OP1521, OP1522, OP1527, OP1528, OP1531) have younger age peaks of 5–16 Ma (comprising 20–76% of the dates). Furthermore, the youngest age peak of these samples decreases in age towards the area of fully reset AFT samples.

We also collected samples (OP1527 and OP1528) close to sample locations with the youngest AFT ages of Brandon et al. (1998), which were reported as incompletely reset samples (with youngest peak ages of 3.9 and 2.3 Ma). In the original publication, only a small number of grains were dated (n=31 and n=12). To improve the statistics of these two samples, we merge our single grain ages with those of Brandon et al. (1998) and obtain more robust age distributions (n=134 and n=80; Table 3). The youngest peak ages of the age populations for the two merged samples are 7.4 Ma and 4.7 Ma (2–4 Myr older than age populations reported by Brandon et al., 1998).

ZHe ages constrain an area of reset ages (4.8–10.2 Ma) in the central, high-topography portion of the mountain range (light grey-shaded area in Fig. 4a). Five of these samples have AFT (5.1–7.8 Ma) and ZHe (4.8–8.9 Ma) ages that overlap within sample errors, implying rapid cooling (and hence fast exhumation) through both systems' closure isotherms. AHe ages of these samples are younger (1.7–3.9 Ma) and do not overlap with AFT ages, indicating that exhumation rates decreased after cooling below the AFT closure isotherm.

Of the seven samples dated with the ZFT method, only sample OP1539 has a fully reset age (12.6 Ma). Together with data from Brandon and Vance (1992) and Stewart and Brandon (2004) this confines reset ZFT samples to a very small area east/southeast of Mt. Olympus, encompassing the headwaters of Elwha and Quinault rivers (area outlined with a red dashed line in Fig. 4a).

4.2 Exhumation histories from thermo-kinematic modelling

Between 13,000–17,800 simulations provide a good fit to the data for each of the seven samples used in the thermo-kinematic modelling (Fig. 5). As expected, the four samples (OP1533, OP1539, OP1551, OP1582; Fig. 5) with overlapping AFT and ZHe ages require fast exhumation rates of >3 km/Myr between 5 Ma and 8 Ma, followed by a reduction to <0.2 km/Myr at 5 Ma or 7 Ma. The reduction of rates for sample OP1573 occurs at ~9

Ma. However, for this sample the AFT age has a larger uncertainty, hence we consider the 5–7 Ma decrease in exhumation rates as a more robust signal. Six of the seven samples (except for sample OP1517) also record an increase in exhumation rates at 2–3 Ma to rates >1 km/Myr.

4.3 Estimating the flux steady-state balance

The calculated volumes of the accretionary influx depend strongly on the incoming sediment thickness (Table 5). In the two-dimensional scenario, volumes vary between ~530 km^3 (for a 1.5 km sediment thickness), ~600 km^3 (for an increasing sediment thickness from 1.5 km to 2.5 km at 2 Ma), and ~1000 km^3 (for a 2.5 km sediment thickness). In the three-dimensional scenario, where accretion is considered along a length of 131 km (cf., Section 3.3.1), volumes vary between ~70,000 km^3 (1.5 km), ~76,000 km^3 (1.5 km to 2.5 km at 2 Ma) and ~130,000 km^3 (2.5 km).

The estimated amount of sediment within the accretionary wedge varies depending on the position within the wedge (Fig. 7). Offshore Vancouver Island, there is 950–1,000 km^3 of sediment within the wedge (Davis and Hyndman, 1989), while on the Olympic Peninsula there is up to ~5,300 km^3 and 3,600 km^3 of sediment within the central and southern parts of the mountain range, respectively.

Our estimates of the denudational outflux vary for the different exhumation rate scenarios (Table 5). In the two-dimensional scenario, the volume of denuded material is 960 km^3 for constant exhumation rates. Estimated volumes increase to 1060–1160 km^3, if an increase in exhumation rates due to Plio-Pleistocene glaciation is considered. In the three-dimensional scenario, estimated volumes range from 72,000 km^3 for constant exhumation rates to 80,000–88,000 km^3 for the exhumation scenario with increasing rates.

5 Discussion

In the following, implications of the above described observations will be discussed in order to assess the flux steady-state balance between accretionary influx and denudational outflux within the Olympic Mountains. To do that, it is pivotal to have an understanding of both temporal and spatial variations in exhumation of the Olympic Mountains. First, we elaborate on results from thermochronometric dating, including the applicability of age-elevation relationships to reconstruct exhumation rates in the Olympic Mountains (Section 5.1). Second, we analyse the general pattern of exhumation based on the spatial distribution of cooling ages (Section 5.2). Third, we link thermochronometric cooling ages with thermo-kinematic modelling, which reveals the temporal evolution of exhumation rates (Section 5.3). Fourth, we discuss the outcome of our qualitative and quantitative assessment of flux steady-state in the Olympic Mountains (Section 5.4). Finally, in Section 5.5, we elaborate on the limitations of the different approaches.

5.1 Age-elevation relationships

The cooling ages of samples collected from a quasi-vertical elevation profile (e.g., Fitzgerald et al., 1993; Reiners et al., 2003) can be analysed by looking at the age-elevation relationship. Often, the purpose is to determine an apparent exhumation rate by fitting a line through the data points when ages are positively correlated with elevation. However, the prerequisite for this approach is that, over the lateral extent of the sampled transect, no significant gradient in exhumation rates exists. This is not necessarily given in the Olympic Mountains (Michel et al., 2018; see also Fig. 2e) and the new data represent this complication (Figs. 4b–d).

At Mt. Olympus, the AHe and ZHe age-elevation relationships do show a positive correlation, suggesting fast exhumation rates of ~1 km/Myr between ~8 and 2 Ma (Fig. 4b). The Mt. Anderson age-elevation relationship for AHe shows a break in slope at ~1400 m and decreasing AHe ages at higher elevations, and the large

uncertainties of the ZHe ages limit an interpretation (Fig. 4c). While such an 'inverse' age-elevation relationship could be caused by a change in relief (Braun, 2002), we interpret it to be a result of the strong spatial variation in exhumation rates along the horizontal distance of the transect (e.g., rates increase from 0.25 km/Myr to 0.9 km/Myr over a horizontal distance of 15–20 km; Fig. 2e). In the case of the Blue Mountain transect (Fig. 4d), we relate the non-correlation of AHe ages and elevation to an incomplete resetting of the AHe system in this area. Here, some samples experienced high enough temperatures to start, or even complete, resetting of the AHe thermochronometric system, causing the observed variability in AHe ages. All ZHe ages from this transect are unreset, corroborating that this part of the Olympic Mountains has not experienced high temperatures, compared to the other transects. Indeed, the Blue Mountain transect belongs to the Coast Range Terrane (CRT), which is at a structurally higher level compared to the accretionary wedge (Fig. 1c). In summary, the age-elevation plots support previous results of strong lateral variations in exhumation and incomplete resetting of thermochronometer systems in the outer part of the mountain range.

5.2 Pattern of exhumation

A well-constrained spatial pattern of exhumation is needed for calculating the denudational outflux. Looking at the spatial distribution of thermochronometric cooling ages provides qualitative information about the pattern of exhumation. In general, the distribution of thermochronometric ages indicates that in the Olympic Mountains the magnitude of exhumation increases from the coast to the centre. As discussed above, areas belonging to the Coast Range Terrane (close to the coast or the Blue Mountain area, where unreset AHe ages can be found, Fig. 2a) correspond to the structurally highest parts within the range (Fig. 1c) and were not sufficiently reheated to reset the AHe system. Assuming a geothermal gradient typical for the Cascadia Subduction Zone of ~20 °C/km (Booth-Rea et al., 2008; Hyndman and Wang, 1993) and an AHe closure temperature of ~60–70°C,

the cumulative exhumation magnitude since onset of exhumation at ~18 Ma cannot have been greater than 2–3 km.

The aerial exposure of the accretionary wedge (the Olympic Structural Complex, Fig. 1c) records exhumation from greater depths. Here, all samples yield reset AHe ages, requiring a minimum exhumation depth of 2–3 km. In the centre of the mountain range (encompassing the headwaters of Hoh, Queets, Quinault and Elwha rivers; Fig. 1b) the area of reset AFT ages approximately overlaps with the area of reset ZHe ages (Fig. 4a), requiring deeper exhumation, compared to the coastal part of the Olympic Structural Complex.

The area east/south-east of Mt. Olympus (corresponding to the area of reset ZFT samples, Fig. 4a) has been exhumed from the greatest depths within the Olympic Mountains. For an average ZFT closure temperature of ~240 °C (Ehlers, 2005) and the above geothermal gradient this corresponds to a maximum exhumation from depths of 10–12 km, confirming previous estimates (Brandon and Calderwood, 1990; Brandon and Vance, 1992).

In summary, the central, high topography part of the mountain range corresponds to the most deeply exhumed part. This corroborates the exhumation rate pattern (Fig. 2e) suggested by Michel et al. (2018), the pattern of denudation rates based on cosmogenic nuclide dating (Adams and Ehlers, 2018), and results from topographic analysis (Adams and Ehlers, 2017), which all suggest that most of the exhumation/denudation occurs at this location. Hence, we use this pattern for the calculation of the denudational outflux.

5.3 Temporal variations in exhumation

Our new thermo-kinematic modelling revealed temporal variations in exhumation rates in the Olympic Mountains (Fig. 5). The decrease of exhumation rates at 5–7 Ma can be readily explained by the reduction in plate convergence rate and the change in convergence direction (Fig. 8). A Pacific-wide reorganization of plate movement at 5.9 Ma has been suggested (Wilson, 2002), and rapid uplift of the Oregon Coast Range at 6–7.5 Ma

with a subsequent cessation in uplift has also been attributed to variations in the plate subduction parameters (McNeill et al., 2000). Furthermore, the volcanic record of the Cascadia Subduction Zone shows temporal variations, where the strongest volcanic activity lasted from 25 Ma until 18 Ma (du Bray and John, 2011). A period of volcanic quiescence, lasting from 17 Ma until 8 Ma, was then followed by increased activity, starting at ~7 Ma. A change in the stress field of the Cascadia Subduction Zone occurred at 7 Ma, which likely also affected the composition of the magmatism (Priest, 1990). Therefore, we interpret our observed 5–7 Ma drop in exhumation rates in the Olympic Mountains as a response to changes in the plate tectonic conditions.

In contrast, the increase in exhumation rates at ~2 Ma indicates a response to climatic rather than tectonic changes. As previously suggested by Michel et al. (2018), increased denudation due to the heavy glaciation of the mountain range led to an increase in exhumation rates by 50–150%, starting at 2–3 Ma. Our study corroborates these findings and shows that the observed young AHe ages require a recent increase in exhumation rates from slower rates (<0.2 km/Myr) lasting from ~7 Ma until ~2 Ma. Glaciation of the North American continent commenced at 2.7 Ma (Haug et al., 2005) and the oldest glacial deposits within the Olympics could be as old as 2 Ma (Easterbrook, 1986), overlapping with our modelled increase in rates at ~2 Ma. Due to the strong spatial variation of the Pleistocene equilibrium line altitude within the Olympic Mountains (Porter, 1964), glacial erosion likely also varied spatially, which could explain the different magnitude in increase of exhumation rates suggested for the different samples. Increased offshore sedimentation related to glacially eroded sediment affected the deformational style of the offshore wedge leading to formation of west-ward dipping thrust faults, which changed at ~1.5 Ma (Adam et al., 2004; Flueh et al., 1998; Gutscher et al., 2001).

Taken together, these observations indicate that temporal variations in exhumation rates within the Olympic Mountains are subject to both changes in the tectonic and climatic conditions (as summarized in Fig. 8). The implication of these variations should be considered for the flux steady-state assessment.

5.4 Flux steady-state in the Olympic Mountains

5.4.1 A qualitative perspective

Several variables that affect both the accretionary influx and the denudational outflux show temporal variations. Exhumation rates decrease at 5–7 Ma and increase at ~2 Ma (Fig. 8) and since exhumation is primarily controlled by denudation, we equate these variations in exhumation with variations in the denudational outflux. According to the model of Doubrovine and Tarduno (2008), the plate subduction velocity decreased at ~6 Ma (see Fig. 6b) after an earlier major decrease at ~25 Ma, causing a decrease in the accretionary influx. Conversely, the accretionary influx increased significantly during the Quaternary due to high offshore sedimentation rates and increased sediment thicknesses as a result of effective glacial erosion on the North American continent (i.e., 50–70 % of the present-day sediment thickness on the subducting Juan de Fuca Plate consists of Quaternary-aged sediments, Table 1 and Fig. 3).

It follows that, qualitatively, both influx and outflux vary through time and are heavily influenced by the Plio-Pleistocene glaciation, which increased denudation rates and offshore sedimentation rates. However, we cannot quantitatively constrain whether variations in the influx and outflux on these short timescales (2–3 Myr) balance each other (and the system would still be in a flux steady-state). Interestingly, measured denudation rates based on cosmogenic nuclide dating (temporally integrating over the Holocene) suggest that modern denudation rates have not been significantly influenced by Plio-Pleistocene glaciation, but are mostly driven by tectonic rock uplift (Adams and Ehlers, 2018). The Holocene accretionary influx, however, is still affected by the increased sediment thickness since the onset of glaciation. Hence, the current accretionary influx seems to exceed the denudational outflux in the Olympic Mountains.

5.4.2 A quantitative perspective

Here, we discuss the quantitative assessment of influx and outflux for the last 14 Myr (Table 5), the time since when the Olympic Mountains are supposed to be in flux steady-state (Batt et al., 2001; Brandon et al., 1998). In the two-dimensional scenario (cf., Figs. 6a, d, and e), the accretionary influx (~1000 km^3) only balances the denudational outflux (1060–1160 km^3), if an incoming sediment thickness of 2.5 km is assumed for the 14 Myr period. Although the present-day sediment thickness at the deformation front is ~2.5 km offshore the Olympic Mountains (Fig. 3), the sediment thickness during pre-Quaternary times is difficult to constrain, but must have been less given that at present, 50–70% of the sediment thickness consists of Quaternary sediments. Assuming a more realistic scenario, where the sediment thickness increases from 1.5 km to 2.5 km at 2 Ma, yields an accretionary influx of only ~600 km^3, which is ~50% of the denudational outflux. This suggests that the two-dimensional scenario is an oversimplification and the excess in outflux along the considered orogen perpendicular profile may be compensated by an excess of influx at other locations or a smaller amount of outflux outside the two-dimensional profile.

In the three-dimensional scenario (Figs. 6a and d), the spatial exhumation rate pattern is integrated to infer the denudational outflux (Fig. 6d). Assuming an increase in sediment thickness at 2 Ma yields an accretionary volume (~76,000 km^3) close to the denudational outflux (80,000–88,000 km^3). Contrary to the two-dimensional scenario, assuming a maximum sediment thickness of 2.5 km for the 14 Myr period yields an accretionary volume of ~130,000 km^3, which cannot be reconciled with our denudational outflux (Table 5). Hence, flux steady-state is a plausible assumption over longer timescales (i.e., 14 Myr), if accretion and denudation are considered over large areas in three dimensions. This highlights that the spatial geometry considered for the flux analysis is crucial. Contrary to an earlier study, which suggested flux steady-state in the Olympic Mountains based on a two-dimensional geometry (using a constant sediment thickness of 2.5 km during

the 14 Myr period; Batt et al., 2001), we suggest that a three-dimensional geometry must be considered in order to obtain flux steady-state. In general, it is important to consider the spatial geometry inherent to the flux analysis in areas with spatially variable exhumation rates, like in the Olympic Mountains.

Sediment volumes integrated along the cross-sections (Fig. 7) also provide an interesting perspective on the accretionary influx in the Olympic Mountains. These volumes are not directly comparable with the influx/outflux volumes discussed above (calculated from 14–0 Ma), because the sediment contained within the cross-sections (Fig. 7) records accretion since the ~40 Ma onset of subduction (Brandon et al., 1998; du Bray and John, 2011). Furthermore, these estimates are minimum volumes, because the amount of material that has been eroded during the 40 Myr period is not considered. Nevertheless, the amount of sediment currently residing in the accretionary wedge is variable along strike of the subduction zone (1000–5400 km^3) and is highest below the central part of the Olympic Mountains (Fig. 7). This requires that parameters affecting the accretionary influx (like plate subduction velocity or sediment thickness) are highly variable over short distances (Profile 1 and Profile 2 are only 50 km apart; Fig. 7). Another explanation might be that considering accretion only perpendicular to the deformation is an oversimplification and another velocity component also contributes to material transport (see Section 5.5). This is in accordance with the conclusion drawn above that considering flux steady-state in a two-dimensional scenario (as it is done with the cross-sections) leads to ambiguous results.

In summary, the assessment of flux steady-state in the Olympic Mountains is non-trivial and many scenarios are possible. From a qualitative viewpoint, flux steady-state is probably not achieved on short timescales (few Myr), because the thickness of incoming sediment, plate subduction velocity, and exhumation rates show strong temporal variations on timescales of 2–3 Myr. From a quantitative viewpoint, influx and outflux volumes equate each other over longer timescales (i.e., 14 Myr), if influx and outflux are considered in three dimensions.

5.5 Restrictions and limitations of our approaches

In the sections above, we discussed exhumation in the Olympic Mountains and the results from our flux calculations. In the following section, we want to elaborate on possible restrictions or limitations in our approaches.

With our 1D modelling, we revealed strong temporal variations in exhumation rates (Fig. 5) related both to variations in tectonic and climatic conditions (Fig. 8). However, two of our modelled samples (OP1513 and OP1517) do not display the decrease in exhumation rates at ~5–7 Ma. These are from the Elwha valley (Fig. 4), in contrast to the five samples displaying the decrease, which are located in the western part of the mountain range. This suggests that the response of the orogenic wedge to a variation in the tectonic conditions affects only parts of the wedge and might be controlled by discrete structures. Further sampling and thermochronometric dating would be required to localize possible faults. Furthermore, this places a limitation on the application of a refined 3D model, because it requires to constrain parameters such as fault location or displacement on these faults. Besides the importance of single structures, the general pattern of deformation in the Olympic Mountains should still be viewed as controlled by the geometry of the subducted plate (Adams and Ehlers, 2017; Adams and Ehlers 2018; Brandon and Calderwood, 1990; Michel et al., 2018).

Regarding our flux analysis, we based our calculations on the volume of accreted sediment within a certain time (governed by the sediment thickness and the plate convergence rate) and the amount of denuded material (governed by the exhumation rates). During our influx calculations, we did not distinguish between different modes of accretion, such as frontal accretion or underplating. Batt et al. (2001) concluded that most accretion occurs at the front of the wedge. However, a recent seismic study showed that sedimentary underplating is taking place below the Olympic Mountains (Calvert et al., 2011). For our approach, the mechanism of accretion does not matter, because we are only interested in whether mass is balanced over the entire wedge and

not at a specific point. As indicated, this is a limitation of our approach and might lead to an overestimation of the actual influx volume, because we do not account for the amount of sediment transported towards the mantle.

Flux steady-state implies that the outflux from and influx into a mountain range balance each other. An inherent assumption is often that the outflux from the mountain range controls the influx, so that in the case of an accretionary wedge, sediment is basically recycled. As we described in Section 2.3 of the manuscript, the sediment currently entering the accretionary wedge of the Cascadia Subduction Zone is a mixture of sediment from different source regions (e.g., Olympic Mountains, Vancouver Island, Canadian Cordillera and in case of the Astoria fan the interior USA, Fig. 3). With the increased detrital input from the Cordilleran Ice Sheet from outside the Olympic Mountains, this effect became particularly pronounced since the onset of Plio-Pleistocene glaciation. Hence, our influx/outflux calculations for the Olympic Mountains do not represent a closed system, where the influx into the Olympic Mountains is solely controlled by the outflux out of the system. However, our calculations indicate that on long timescales (i.e., over 14 Myr) flux steady-state is attained, which might seem surprising given that the sediment thickness is governed by contributions from different source regions. We suspect that processes during sediment deposition, like redistribution by turbidity currents and redeposition in more proximal parts of the Juan de Fuca Plate, play an important role in the final sediment budget. As a consequence, the amount of sediment denuded from the Olympic Peninsula in a given time period (the outflux) is dispersed as it enters the ocean, so that for the same time period only a fraction of the sediment thickness (governing the influx) is composed of material originating from the Olympic Peninsula.

Variations in the geometry or extent of the accretionary wedge were also not included in our flux analysis. Since onset of subduction at the Cascadia Subduction Zone with the present geometry at ~40 Ma, the wedge must have grown over time in order to attain its present shape. As soon as a balance between accretion and erosion is established, the shape of an orogenic wedge remains constant, controlled by its critical taper (e.g.,

Davis et al., 1983). However, Adam et al. (2004) showed that the Cascadia accretionary wedge responded to increased offshore sedimentation during the Quaternary by development of west-ward dipping thrust faults, shifting the deformation front further seawards thereby increasing the extent and volume of the wedge. An important parameter contributing to the shape of the accretionary wedge is the angle of subduction, which is flatter below the Olympic Mountains (compared to areas north or south) due to the bend in the subducted slab (Fig. 1a). A reason hypothesized for bending the subducting slab is extension in the Basin and Range Province, starting in the middle Miocene (Brandon and Calderwood, 1990). All these points indicate that parameters controlling the size and volume of the accretionary wedge are both spatially and temporally variable. However, we cannot account for all of these circumstances in our flux calculations, because they are difficult to constrain quantitatively from available observations. Furthermore, because we based our flux calculations only on volumes of accreted or eroded material over the 14 Myr period, a comparison between these two volumes itself should not depend on a change in the shape or extent of the accretionary wedge.

As we pointed out in Section 5.4.2 the assumed geometry for the flux balance is crucial. However, both in the two- and three-dimensional scenarios, we only considered the deformation front-perpendicular velocity component for our influx calculations. The different sediment volumes contained in the reported cross-sections (Fig. 7) could indicate that on long timescales additional velocity components must be considered. We can only speculate that margin-parallel transport, which is a contentious topic at the Cascadia Subduction Zone (e.g., Batt et al., 2001; McCrory, 1996; Wang, 1996), also contributes to the accretionary influx. Present-day GPS velocities corroborate this hypothesis, indicating northward movement of coastal areas south of the Olympic Mountains (e.g., McCaffrey et al., 2013; Wells and McCaffrey, 2013).

To summarize, several parameters like the location of faults within the orogenic wedge, the sediment source region, the temporal evolution of the wedge geometry or margin parallel transport are difficult to constrain

from current observations. Although we emphasized that not all of these parameters affect our flux analysis, further knowledge of these will refine the current understanding of steady-state in the Olympic Mountains.

6 Conclusion

Our new data set of multi-dated thermochronometer bedrock samples together with thermo-kinematic modelling suggests that several mechanisms contribute to the evolution of the Olympic Mountains. Modelling of the observed AHe, AFT, ZHe, and ZFT ages shows that variations in both tectonic and climatic conditions result in temporal variations of exhumation rates. We revealed a hitherto unnoticed response of exhumation to the tectonic signal (a reduction in plate convergence rate causing a drop in exhumation rates), which can also be observed in other parts of the Cascadia Subduction Zone. Plio-Pleistocene glaciation of the Olympic Mountains led to increased denudation, resulting in increased exhumation rates.

Our approach of assessing flux steady-state in the Olympic Mountains by estimating the material influx and outflux independently from each other is promising, but yields ambiguous results. The observed temporal variations in exhumation rate require a variation in the denudational outflux. Likewise, the accretionary influx is also temporally variable, because the plate subduction velocity and incoming sediment thickness are variable through time. Qualitatively, this suggests that flux steady-state is perturbed on short timescales by variations in the tectonic or climatic conditions. Our quantitative calculations of the influx and outflux show flux steady-state may be achievable over long timescales (i.e., 14 Myr), but that it is important to consider whether flux steady-state is assessed in two or three dimensions. Contrary to a previous flux steady-state analysis in the Olympic Mountains, our calculated influx and outflux volumes only balance each other, if a three-dimensional geometry is considered.

This study demonstrates the timescale (10^5–10^6 vs. 10^7 Myr) and spatial (two- or three-dimensional) dependence of a steady-state assessment in an orogenic wedge, an outcome that can also be considered for other mountain ranges. Furthermore, the tremendous effect of the Plio-Pleistocene glaciation is demonstrated, which is capable of significantly perturbing the development of an orogenic wedge, where both the influx and outflux are affected. Because the spatial geometry used for assessing flux steady-state is crucial, more work is needed to constrain the role of material transport parallel to the deformation front. Such studies will lead to a better understanding of the development of orogenic wedges situated in a complex tectonic setting like the Olympic Mountains.

Acknowledgements

This work was funded by a European Research Council (ERC) Consolidator Grant (615703) to Todd Ehlers. During field work, we had invaluable help and assistance by Holger Sprengel, William Baccus, Jerry Freilich, Roger Hofmann, and the Olympic National Park rangers. We acknowledge Matthias Nettesheim for sharing the code used for evaluation of the tectonic plate reconstruction model, and the help of Willi Kappler during Pecube modelling. The comments of two anonymous referees helped to improve this manuscript.

References

Adam, J., Klaeschen, D., Kukowski, N. and Flueh, E.: Upward delamination of Cascadia Basin sediment infill with landward frontal accretion thrusting caused by rapid glacial age material flux, Tectonics, 23(3), doi:10.1029/2002TC001475, 2004.

Adams, B. A. and Ehlers, T. A.: Deciphering topographic signals of glaciation and rock uplift in an active orogen: a case study from the Olympic Mountains, USA: Signals of glaciation and rock uplift in the Olympic Mountains, Earth Surface Processes and Landforms, 42(11), 1680–1692, doi:10.1002/esp.4120, 2017.

Adams, B. A. and Ehlers, T. A.: Tectonic controls of Holocene erosion in a glaciated orogen, Earth Surf. Dynam., 6(3), 595–610, doi:10.5194/esurf-6-595-2018, 2018.

Adams, B. A., Hodges, K. V., Whipple, K. X., Ehlers, T. A., van Soest, M. C. and Wartho, J.: Constraints on the tectonic and landscape evolution of the Bhutan Himalaya from thermochronometry: Late Cenozoic Evolution of Bhutan, Tectonics, 34(6), 1329–1347, doi:10.1002/2015TC003853, 2015.

Batt, G. E., Brandon, M. T., Farley, K. A. and Roden-Tice, M.: Tectonic synthesis of the Olympic Mountains segment of the Cascadia wedge, using two-dimensional thermal and kinematic modeling of thermochronological ages, J. Geophys. Res., 106(B11), 26731–26746, doi:10.1029/2001JB000288, 2001.

Bendick, R. and Ehlers, T. A.: Extreme localized exhumation at syntaxes initiated by subduction geometry, Geophys. Res. Lett., 41(16), 2014GL061026, doi:10/f6kfqz, 2014.

Bernard, T., Steer, P., Gallagher, K., Szulc, A., Whitham, A. and Johnson, C.: Evidence for Eocene–Oligocene glaciation in the landscape of the East Greenland margin, Geology, 44(11), 895–898, 2016

Berger, A. L., Gulick, S. P. S., Spotila, J. A., Upton, P., Jaeger, J. M., Chapman, J. B., Worthington, L. A., Pavlis, T. L., Ridgway, K. D., Willems, B. A. and McAleer, R. J.: Quaternary tectonic response to intensified glacial erosion in an orogenic wedge, Nature Geoscience, 1(11), 793–799, doi:10.1038/ngeo334, 2008.

Booth, D. B., Troost, K. G., Clague, J. J. and Waitt, R. B.: The Cordilleran Ice Sheet, in Developments in Quaternary Sciences, vol. 1, pp. 17–43, Elsevier, 2003.

Booth-Rea, G., Klaeschen, D., Grevemeyer, I. and Reston, T.: Heterogeneous deformation in the Cascadia convergent margin and its relation to thermal gradient (Washington, NW USA), Tectonics, 27(4), doi:10.1029/2007TC002209, 2008.

Brandon, M. T.: Decomposition of fission-track grain-age distributions, American Journal of Science, 292(8), 535–564, 1992.

Brandon, M. T.: Probability density plot for fission-track grain-age sample, Radiation Measurements, 26, 663–676, 1996.

Brandon, M. T. and Calderwood, A. R.: High-pressure metamorphism and uplift of the Olympic subduction complex, Geology, 18(12), 1252, doi:10.1130/0091-7613(1990)018<1252:HPMAUO>2.3.CO;2, 1990.

Brandon, M. T. and Vance, J. A.: Tectonic evolution of the Cenozoic Olympic subduction complex, Washington State, as deduced from fission track ages for detrital zircons, American Journal of Science, 292(8), 565–636, doi:10.2475/ajs.292.8.565, 1992.

Brandon, M. T., Roden-Tice, M. K. and Garver, J. I.: Late Cenozoic exhumation of the Cascadia accretionary wedge in the Olympic Mountains, northwest Washington State, Geological Society of America Bulletin, 110(8), 985–1009, doi:10.1130/0016-7606(1998)110<0985:LCEOTC>2.3.CO;2, 1998.

Braun, J.: Estimating exhumation rate and relief evolution by spectral analysis of age–elevation datasets, Terra Nova, 14(3), 210–214, 2002.

Braun, J.: Pecube: a new finite-element code to solve the 3D heat transport equation including the effects of a time-varying, finite amplitude surface topography, Computers & Geosciences, 29(6), 787–794, doi:10.1016/S0098-3004(03)00052-9, 2003.

du Bray, E. A. and John, D. A.: Petrologic, tectonic, and metallogenic evolution of the Ancestral Cascades magmatic arc, Washington, Oregon, and northern California, Geosphere, 7(5), 1102–1133, 2011.

Calvert, A. J., Preston, L. A. and Farahbod, A. M.: Sedimentary underplating at the Cascadia mantle-wedge corner revealed by seismic imaging, Nature Geosci., 4(8), 545–548, doi:10.1038/ngeo1195, 2011.

Carpentier, M., Weis, D. and Chauvel, C.: Fractionation of Sr and Hf isotopes by mineral sorting in Cascadia Basin terrigenous sediments, Chemical Geology, 382, 67–82, doi:10.1016/j.chemgeo.2014.05.028, 2014.

Clague, J. J. and James, T. S.: History and isostatic effects of the last ice sheet in southern British Columbia, Quaternary Science Reviews, 21(1), 71–87, 2002.

Clowes, R. M., Brandon, M. T., Green, A. G., Yorath, C. J., Brown, A. S., Kanasewich, E. R. and Spencer, C.: LITHOPROBE-southern Vancouver Island: Cenozoic subduction complex imaged by deep seismic reflections, Canadian Journal of Earth Sciences, 24(1), 31–51, 1987.

Davis, D., Suppe, J. and Dahlen, F. A.: Mechanics of fold-and-thrust belts and accretionary wedges, J. Geophys. Res., 88(B2), 1153–1172, 1983.

Davis, E. E. and Hyndman, R. D.: Accretion and recent deformation of sediments along the northern Cascadia subduction zone, Geological Society of America Bulletin, 101(11), 1465–1480, 1989.

Doubrovine, P. V. and Tarduno, J. A.: A revised kinematic model for the relative motion between Pacific oceanic plates and North America since the Late Cretaceous, Journal of Geophysical Research, 113(B12), doi:10.1029/2008JB005585, 2008.

Easterbrook, D. J.: Stratigraphy and chronology of quaternary deposits of the Puget Lowland and Olympic Mountains of Washington and the Cascade Mountains of Washington and Oregon, Quaternary Science Reviews, 5, 145–159, doi:10.1016/0277-3791(86)90180-0, 1986.

Eddy, M. P., Clark, K. P. and Polenz, M.: Age and volcanic stratigraphy of the Eocene Siletzia oceanic plateau in Washington and on Vancouver Island, Lithosphere, 9(4), 652–664, doi:10.1130/L650.1, 2017.

Ehlers, T. A.: Computational Tools for Low-Temperature Thermochronometer Interpretation, Reviews in Mineralogy and Geochemistry, 58(1), 589–622, doi:10.2138/rmg.2005.58.22, 2005.

Ehlers, T. A., Farley, K. A., Rusmore, M. E. and Woodsworth, G. J.: Apatite (U-Th)/He signal of large-magnitude accelerated glacial erosion, southwest British Columbia, Geology, 34(9), 765, doi:10.1130/G22507.1, 2006.

Falkowski, S. and Enkelmann, E.: Upper-crustal cooling of the Wrangellia composite terrane in the northern St. Elias Mountains, western Canada, Lithosphere, 8(4), 359–378, doi:10.1130/L508.1, 2016.

Falkowski, S., Enkelmann, E. and Ehlers, T. A.: Constraining the area of rapid and deep-seated exhumation at the St. Elias syntaxis, Southeast Alaska, with detrital zircon fission-track analysis, Tectonics, 33(5), 597–616, doi:10.1002/2013TC003408, 2014.

Farley, K. A.: (U-Th)/He Dating: Techniques, Calibrations, and Applications, Reviews in Mineralogy and Geochemistry, 47(1), 819–844, doi:10.2138/rmg.2002.47.18, 2002.

Fitzgerald, P. G., Stump, E. and Redfield, T. F.: Late Cenozoic uplift of Denali and its relation to relative plate motion and fault morphology, Science, 259, 497–497, 1993.

Flueh, E. R., Fisher, M. A., Bialas, J., Childs, J. R., Klaeschen, D., Kukowski, N., Parsons, T., Scholl, D. W., ten Brink, U. and Tréhu, A. M.: New seismic images of the Cascadia subduction zone from cruise SO108—ORWELL, Tectonophysics, 293(1), 69–84, 1998.

Galbraith, R. F.: Statistics for fission track analysis, CRC Press., 2005.

Gallagher, K., Brown, R. and Johnson, C.: FISSION TRACK ANALYSIS AND ITS APPLICATIONS TO GEOLOGICAL PROBLEMS, Annu. Rev. Earth Planet. Sci., 26(1), 519–572, doi:10/cj5xp8, 1998.

Glotzbach, C., van der Beek, P., Carcaillet, J. and Delunel, R.: Deciphering the driving forces of erosion rates on millennial to million-year timescales in glacially impacted landscapes: An example from the Western Alps, Journal of Geophysical Research: Earth Surface, 118(3), 1491–1515, doi:10.1002/jgrf.20107, 2013.

Gulick, S. P. S., Jaeger, J. M., Mix, A. C., Asahi, H., Bahlburg, H., Belanger, C. L., Berbel, G. B. B., Childress, L., Cowan, E., Drab, L., Forwick, M., Fukumura, A., Ge, S., Gupta, S., Kioka, A., Konno, S., LeVay, L. J., März, C., Matsuzaki, K. M., McClymont, E. L., Moy, C., Müller, J., Nakamura, A., Ojima, T., Ribeiro, F. R., Ridgway, K. D., Romero, O. E., Slagle, A. L., Stoner, J. S., St-Onge, G., Suto, I., Walczak, M. D., Worthington, L. L., Bailey, I., Enkelmann, E., Reece, R. and Swartz, J. M.: Mid-Pleistocene climate transition drives net mass loss from rapidly uplifting St. Elias Mountains, Alaska, Proceedings of the National Academy of Sciences, 112(49), 15042–15047, doi:10.1073/pnas.1512549112, 2015.

Gutscher, M.-A., Klaeschen, D., Flueh, E. and Malavieille, J.: Non-Coulomb wedges, wrong-way thrusting, and natural hazards in Cascadia, Geology, 29(5), 379–382, 2001.

Han, S., Carbotte, S. M., Canales, J. P., Nedimović, M. R., Carton, H., Gibson, J. C. and Horning, G. W.: Seismic reflection imaging of the Juan de Fuca plate from ridge to trench: New constraints on the distribution of faulting and evolution of the crust prior to subduction, Journal of Geophysical Research: Solid Earth, 121(3), 1849–1872, doi:10.1002/2015JB012416, 2016.

Haug, G. H., Ganopolski, A., Sigman, D. M., Rosell-Mele, A. and others: North Pacific seasonality and the glaciation of North America 2.7 million years ago, Nature, 433(7028), 821, 2005.

Hayes, G. P., Wald, D. J. and Johnson, R. L.: Slab1.0: A three-dimensional model of global subduction zone geometries:, Journal of Geophysical Research: Solid Earth, 117(B1), doi:10.1029/2011JB008524, 2012.

Herman, F. and Brandon, M.: Mid-latitude glacial erosion hotspot related to equatorial shifts in southern Westerlies, Geology, 43(11), 987–990, doi:10.1130/G37008.1, 2015.

Herman, F., Seward, D., Valla, P. G., Carter, A., Kohn, B., Willett, S. D. and Ehlers, T. A.: Worldwide acceleration of mountain erosion under a cooling climate, Nature, 504(7480), 423–426, doi:10.1038/nature12877, 2013.

Hourigan, J. K., Reiners, P. W. and Brandon, M. T.: U-Th zonation-dependent alpha-ejection in (U-Th)/He chronometry, Geochimica et Cosmochimica Acta, 69(13), 3349–3365, doi:10.1016/j.gca.2005.01.024, 2005.

Hurford, A. J.: Standardization of fission track dating calibration: Recommendation by the Fission Track Working Group of the I.U.G.S. Subcommission on Geochronology, Chemical Geology, 80, 171–178, 1990.

Hyndman, R. D. and Wang, K.: Thermal constraints on the zone of major thrust earthquake failure: The Cascadia Subduction Zone, Journal of Geophysical Research: Solid Earth, 98(B2), 2039–2060, doi:10.1029/92JB02279, 1993.

Hyndman, R. D., Yorath, C. J., Clowes, R. M. and Davis, E. E.: The northern Cascadia subduction zone at Vancouver Island: Seismic structure and tectonic history, Canadian Journal of Earth Sciences, 27(3), 313–329, 1990.

Kiyokawa, S. and Yokoyama, K.: Provenance of turbidite sands from IODP EXP 1301 in the northwestern Cascadia Basin, western North America, Marine Geology, 260(1–4), 19–29, doi:10.1016/j.margeo.2009.01.003, 2009.

Knudson, K. P. and Hendy, I. L.: Climatic influences on sediment deposition and turbidite frequency in the Nitinat Fan, British Columbia, Marine Geology, 262(1–4), 29–38, doi:10.1016/j.margeo.2009.03.002, 2009.

Kulm, L. V. D., von Huene, R., Duncan, J. R., Ingle, J. C., Kling, S. A., Musich, L. F., Piper, D. J. W., Pratt, R. M., Schrader, H.-J., Weser, O. E. and Wise, S. W.: Site 174, edited by L. V. D. Kulm, R. von Huene, J. R. Duncan, J. C. Ingle, S. A. Kling, D. J. W. Piper, R. M. Pratt, H.-J. Schrader, S. W. Wise, L. F. Musich, and O. E. Weser, Initial Reports of the Deep Sea Drilling Project, 18, 97, 1973.

Lease, R. O. and Ehlers, T. A.: Incision into the Eastern Andean Plateau During Pliocene Cooling, Science, 341(6147), 774–776, doi:10.1126/science.1239132, 2013.

Lease, R. O., Haeussler, P. J. and O'Sullivan, P.: Changing exhumation patterns during Cenozoic growth and glaciation of the Alaska Range: Insights from detrital thermochronology and geochronology, Tectonics, 35(4), 934–955, doi:10.1002/2015TC004067, 2016.

Leeman, W. P., Lewis, J. F., Evarts, R. C., Conrey, R. M. and Streck, M. J.: Petrologic constraints on the thermal structure of the Cascades arc, Journal of Volcanology and Geothermal Research, 140(1–3), 67–105, doi:10.1016/j.jvolgeores.2004.07.016, 2005.

Lewis, T. J. and Bentkowski, W. H.: Potassium, Uranium and Thorium Concentrations of Crustal Rocks: a Data File, Open File Report 1744, Geological Survey of Canada, Sidney, 1988.

Lewis, T. J., Bentkowski, W. H., Davis, E. E., Hyndman, R. D., Souther, J. G. and Wright, J. A.: Subduction of the Juan de Fuca Plate: Thermal consequences, Journal of Geophysical Research: Solid Earth, 93(B12), 15207–15225, doi:10.1029/JB093iB12p15207, 1988.

McCaffrey, R., King, R. W., Payne, S. J. and Lancaster, M.: Active tectonics of northwestern U.S. inferred from GPS-derived surface velocities, Journal of Geophysical Research: Solid Earth, 118(2), 709–723, doi:10.1029/2012JB009473, 2013.

McCrory, P. A.: Tectonic model explaining divergent contraction directions along the Cascadia subduction margin, Washington, Geology, 24(10), 929, doi:10.1130/0091-7613(1996)024<0929:TMEDCD>2.3.CO;2, 1996.

McCrory, P. A., Blair, J. L., Waldhauser, F. and Oppenheimer, D. H.: Juan de Fuca slab geometry and its relation to Wadati-Benioff zone seismicity, Journal of Geophysical Research: Solid Earth, 117(B9), doi:10.1029/2012JB009407, 2012.

McNeill, L. C., Goldfinger, C., Kulm, L. D. and Yeats, R. S.: Tectonics of the Neogene Cascadia forearc basin: Investigations of a deformed late Miocene unconformity, Geological Society of America Bulletin, 112(8), 1209–1224, 2000.

Meesters, A. G. C. A. and Dunai, T. J.: A noniterative solution of the (U-Th)/He age equation, Geochemistry, Geophysics, Geosystems, 6(4), doi:10.1029/2004GC000834, 2005.

Michel, L., Ehlers, T. A., Glotzbach, C., Adams, B. A. and Stübner, K.: Tectonic and glacial contributions to focused exhumation in the Olympic Mountains, Washington, USA, Geology, 46(6), 491–494, doi:10/gc8z9w, 2018.

Montgomery, D. R.: Valley formation by fluvial and glacial erosion, Geology, 30(11), 1047–1050, doi:10.1130/0091-7613(2002)030<1047:VFBFAG>2.0.CO;2, 2002.

Montgomery, D. R. and Greenberg, H. M.: Local relief and the height of Mount Olympus, Earth Surface Processes and Landforms, 25(4), 385–396, 2000.

Mullen, E. K., Weis, D., Marsh, N. B. and Martindale, M.: Primitive arc magma diversity: New geochemical insights in the Cascade Arc, Chemical Geology, 448, 43–70, doi:10.1016/j.chemgeo.2016.11.006, 2017.

Mutz, S. G., Ehlers, T. A., Werner, M., Lohmann, G., Stepanek, C. and Li, J.: Estimates of late Cenozoic climate change relevant to Earth surface processes in tectonically active orogens, Earth Surface Dynamics, 6(2), 271–301, doi:10/gc8sbw, 2018.

Pazzaglia, F. J. and Brandon, M. T.: A fluvial record of long-term steady-state uplift and erosion across the Cascadia forearc high, western Washington State, Am. J. Sci., 301(4–5), 385–431, 2001.

Phillips, B. A., Kerr, A. C., Mullen, E. K. and Weis, D.: Oceanic mafic magmatism in the Siletz terrane, NW North America: Fragments of an Eocene oceanic plateau?, Lithos, 274–275, 291–303, doi:10.1016/j.lithos.2017.01.005, 2017.

Porter, S. C.: Composite Pleistocene snow line of Olympic Mountains and Cascade Range, Washington, Geological Society of America Bulletin, 75(5), 477–482, 1964.

Priest, G. R.: Volcanic and tectonic evolution of the Cascade Volcanic Arc, central Oregon, Journal of Geophysical Research: Solid Earth, 95(B12), 19583–19599, doi:10.1029/JB095iB12p19583, 1990.

Prytulak, J., Vervoort, J. D., Plank, T. and Yu, C.: Astoria Fan sediments, DSDP site 174, Cascadia Basin: Hf–Nd–Pb constraints on provenance and outburst flooding, Chemical Geology, 233(3–4), 276–292, doi:10.1016/j.chemgeo.2006.03.009, 2006.

Reiners, P. W., Zhou, Z., Ehlers, T. A., Xu, C., Brandon, M. T., Donelick, R. A. and Nicolescu, S.: Post-orogenic evolution of the Dabie Shan, eastern China, from (U-Th)/He and fission-track thermochronology, American Journal of Science, 303(6), 489–518, 2003.

Reiners, P. W., Spell, T. L., Nicolescu, S. and Zanetti, K. A.: Zircon (U-Th)/He thermochronometry: He diffusion and comparisons with $^{40}Ar/^{39}Ar$ dating, Geochim. Cosmochim. Acta, 68(8), 1857–1887, doi:10.1016/j.gca.2003.10.021, 2004.

Stewart, R. J. and Brandon, M. T.: Detrital-zircon fission-track ages for the "Hoh Formation": implications for late Cenozoic evolution of the Cascadia subduction wedge, Geological Society of America Bulletin, 116(1–2), 60–75, 2004.

Stolar, D., Roe, G. and Willett, S.: Controls on the patterns of topography and erosion rate in a critical orogen, Journal of Geophysical Research, 112(F4), doi:10.1029/2006JF000713, 2007.

Stübner, K., Drost, K., Schoenberg, R., Böhme, M., Starke, J. and Ehlers, T. A.: Asynchronous timing of extension and basin formation in the South Rhodope core complex, SW Bulgaria, and northern Greece, Tectonics, 35(1), 136–159, doi:10.1002/2015TC004044, 2016.

Su, X., Baumann, K. H. and Thiede, J.: Calcareous nannofossils from Leg 168: biochronology and diagenesis, in Proceedings of the Ocean Drilling Program, Scientific Results, vol. 168, pp. 39–50., 2000.

Tabor, R. W. and Cady, W. M.: The structure of the Olympic Mountains, Washington: Analysis of a subduction zone, US Govt. Print. Off., 1978.

Thackray, G. D.: Extensive Early and Middle Wisconsin Glaciation on the Western Olympic Peninsula, Washington, and the Variability of Pacific Moisture Delivery to the Northwestern United States, Quaternary Research, 55(3), 257–270, doi:10.1006/qres.2001.2220, 2001.

Thiede, R. C. and Ehlers, T. A.: Large spatial and temporal variations in Himalayan denudation, Earth and Planetary Science Letters, 371–372, 278–293, doi:10.1016/j.epsl.2013.03.004, 2013.

Thomson, S. N., Brandon, M. T., Tomkin, J. H., Reiners, P. W., Vásquez, C. and Wilson, N. J.: Glaciation as a destructive and constructive control on mountain building, Nature, 467(7313), 313–317, doi:10.1038/nature09365, 2010.

Thomson, S. N., Reiners, P. W., Hemming, S. R. and Gehrels, G. E.: The contribution of glacial erosion to shaping the hidden landscape of East Antarctica, Nat. Geosci., 6(3), 203–207, doi:10.1038/ngeo1722, 2013

Tomkin, J. H. and Roe, G. H.: Climate and tectonic controls on glaciated critical-taper orogens, Earth and Planetary Science Letters, 262(3–4), 385–397, doi:10.1016/j.epsl.2007.07.040, 2007.

Valla, P. G., Shuster, D. L. and van der Beek, P. A.: Significant increase in relief of the European Alps during mid-Pleistocene glaciations, Nature Geosci, 4(10), 688–692, doi:10.1038/ngeo1242, 2011.

Wang, K.: Simplified analysis of horizontal stresses in a buttressed forearc sliver at an oblique subduction zone, Geophys. Res. Lett., 23(16), 2021–2024, doi:10/dz2xxt, 1996.

Wells, R. E. and McCaffrey, R.: Steady rotation of the Cascade arc, Geology, 41(9), 1027–1030, doi:10.1130/G34514.1, 2013.

Wells, R. E., Bukry, D., Friedman, R., Pyle, D., Duncan, R., Haeussler, P. and Wooden, J.: Geologic history of Siletzia, a large igneous province in the Oregon and Washington Coast Range: Correlation to the geomagnetic polarity time scale and implications for a long-lived Yellowstone hotspot, Geosphere, 10(4), 692–719, 2014.

Westbrook, G., Carson, B. and Musgrave, R.: Shipboard Scientific Party, 1994, Initial reports of the Ocean Drilling Program, 146(pt 1), 1994.

Whipple, K. X.: The influence of climate on the tectonic evolution of mountain belts, Nature Geosci., 2(2), 97–104, doi:10.1038/ngeo413, 2009.

Whipple, K. X. and Meade, B.: Orogen response to changes in climatic and tectonic forcing, Earth and Planetary Science Letters, 243(1–2), 218–228, doi:10.1016/j.epsl.2005.12.022, 2006.

Willett, S. D.: Orogeny and orography: The effects of erosion on the structure of mountain belts, J. Geophys. Res., 104(B12), 28957–28981, doi:10.1029/1999JB900248, 1999.

Willett, S. D. and Brandon, M. T.: On steady states in mountain belts, Geology, 30(2), 175–178, doi:10.1130/0091-7613(2002)030<0175:OSSIMB>2.0.CO;2, 2002.

Willett, S. D., McCoy, S. W., Perron, J. T., Goren, L. and Chen, C.-Y.: Dynamic Reorganization of River Basins, Science, 343(6175), 1248765–1248765, doi:10.1126/science.1248765, 2014.

Wilson, D. S.: Confidence intervals for motion and deformation of the Juan de Fuca Plate, Journal of Geophysical Research: Solid Earth, 98(B9), 16053–16071, doi:10.1029/93JB01227, 1993.

Wilson, D. S.: The Juan de Fuca plate and slab: Isochron structure and Cenozoic plate motions, in: The Cascadia Subduction Zone and related subduction systems: seismic structure, intraslab earthquakes and processes, and earthquake hazards, US Geological Survey, Reston, VA., 2002.

Yanites, B. J. and Ehlers, T. A.: Global climate and tectonic controls on the denudation of glaciated mountains, Earth and Planetary Science Letters, 325–326, 63–75, doi:10.1016/j.epsl.2012.01.030, 2012.

Yanites, B. J., Ehlers, T. A., Becker, J. K., Schnellmann, M. and Heuberger, S.: High magnitude and rapid incision from river capture: Rhine River, Switzerland, Journal of Geophysical Research: Earth Surface, 118(2), 1060–1084, doi:10.1002/jgrf.20056, 2013.

Yuan, T., Spence, G. D. and Hyndman, R. D.: Seismic velocities and inferred porosities in the accretionary wedge sediments at the Cascadia margin, Journal of Geophysical Research: Solid Earth, 99(B3), 4413–4427, doi:10/dfwxqf, 1994.

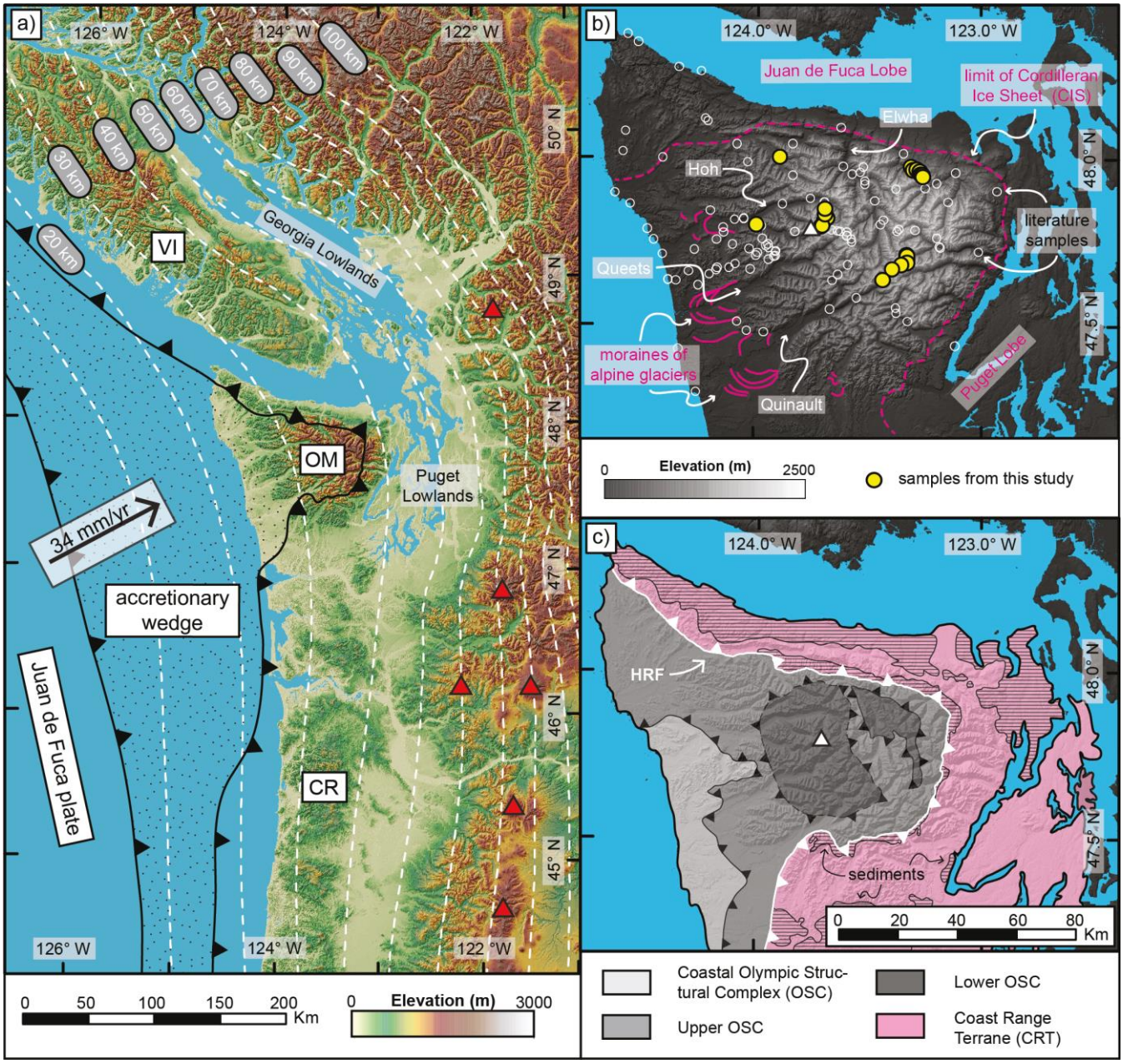

Figure 1: a) Overview map of the Cascadia Subduction Zone, showing the extent of the accretionary wedge. White dashed lines are contour lines for the top of the subducted oceanic plate from the Slab1.0 model (Hayes et al., 2012; McCrory et al., 2012), the black arrow indicates the present-day convergence rate and direction at the latitude of the Olympic Mountains (Doubrovine and Tarduno, 2008), red triangles denote the location of active volcanoes. VI = Vancouver Island, OM = Olympic Mountains, CR = Oregon Coast Range. b) Topography of the Olympic Mountains, major river valleys (Elwha, Hoh, Quinault, Queets) and major Quaternary features are indicated. Limit of the Cordilleran Ice Sheet from Porter (1964), alpine moraines after geologic map of Tabor and Cady (1978). Locations of samples from this study (filled yellow circles) and previous studies (open white circles) are indicated. The white triangle denotes the location of Mt. Olympus. c) Geologic and structural map of the Olympic Mountains after Tabor and Cady (1978) and Brandon et al. (1998). The line pattern indicates the occurrence of sediments within the Coast Range Terrane. HRF = Hurricane Ridge Fault.

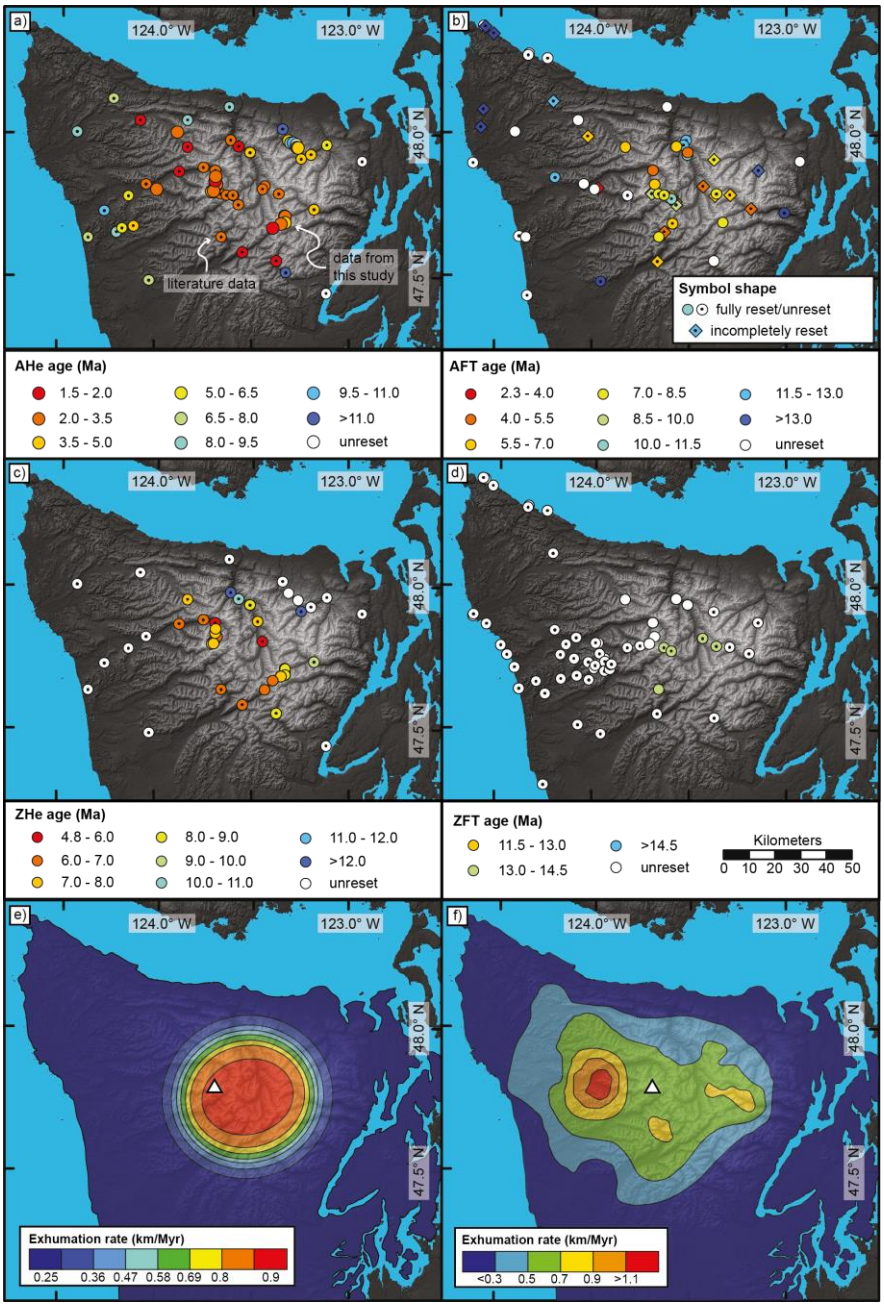

Figure 2: Map of new and previously published thermochronometric ages within the Olympic Mountains for a) AHe, b) AFT, c) ZHe and d) ZFT. Data from literature (Batt et al., 2001; Brandon et al., 1998; Brandon and Vance, 1992; Michel et al., 2018; Stewart and Brandon, 2004) are indicated by circles with black dot. Note that the colour coding of the symbols varies between panels. For AFT literature samples, the different reset states (fully reset, incompletely reset and unreset) are indicated by symbol shape. Maps of exhumation rates, as suggested by (e) Michel et al. (2018) and (f) Brandon et al. (1998). The white triangle denotes the location of Mt. Olympus.

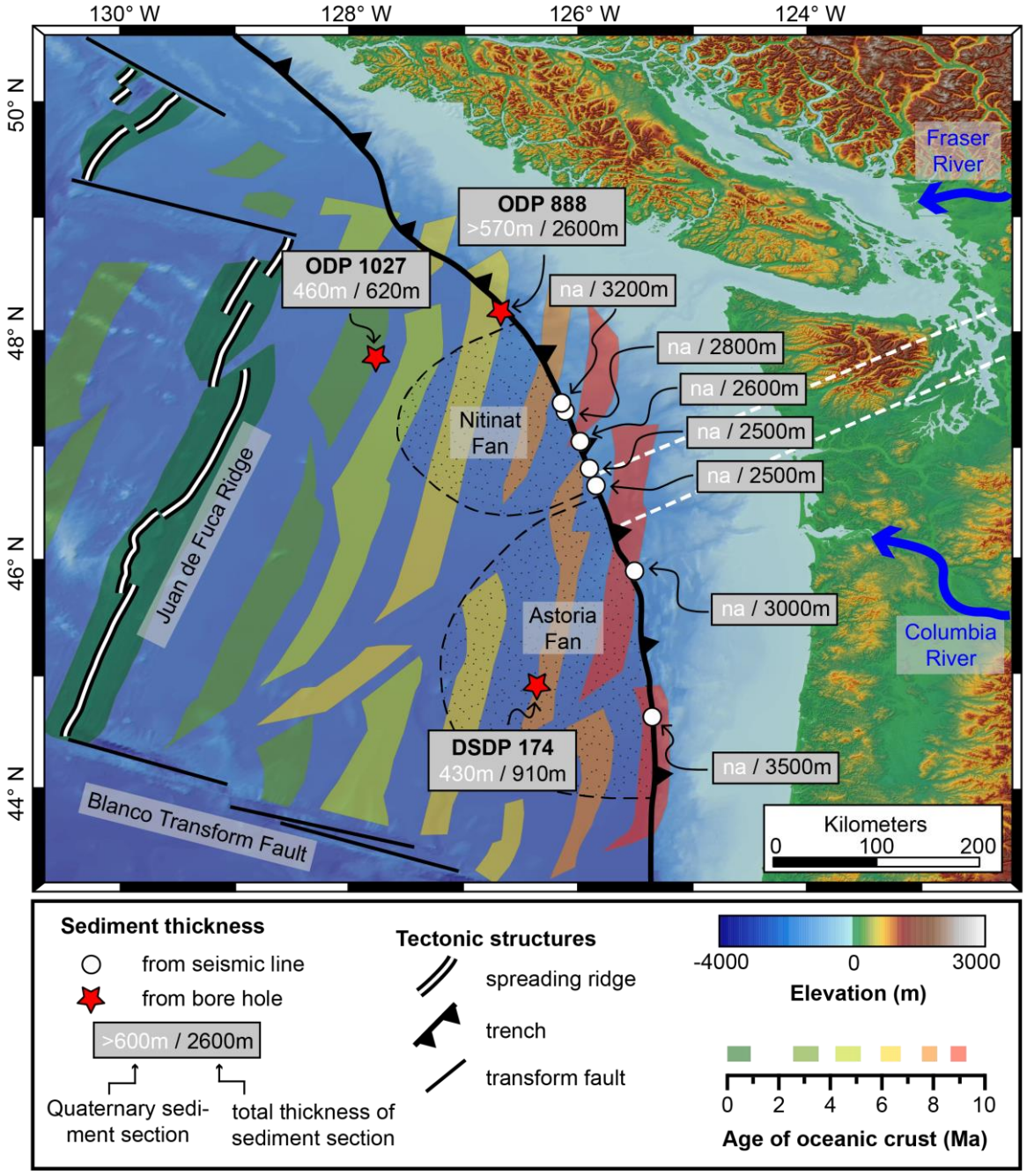

Figure 3: Map of the Cascadia Subduction Zone, showing the age of the oceanic crust (Wilson, 1993) and sediment thickness, estimated from sediment cores of the ocean drilling programs (holes ODP 888, OPD 1027 and DSDP 174) and seismic studies (Adam et al., 2004; Booth-Rea et al., 2008; Han et al., 2016). The amount of Quaternary sediment material estimated from cores is also included (Kulm et al., 1973; Su et al., 2000; Westbrook et al., 1994), more information about the drill cores is provided in Table 1. The locations of two major submarine fans (Nitinat Fan and Astoria Fan) are indicated by the dotted pattern. The Fraser and Columbia rivers are the main modern sediment sources for Nitinat and Astoria fans, respectively. White, dashed lines indicate the position of cross-sections presented in this study (cf., Fig. 7).

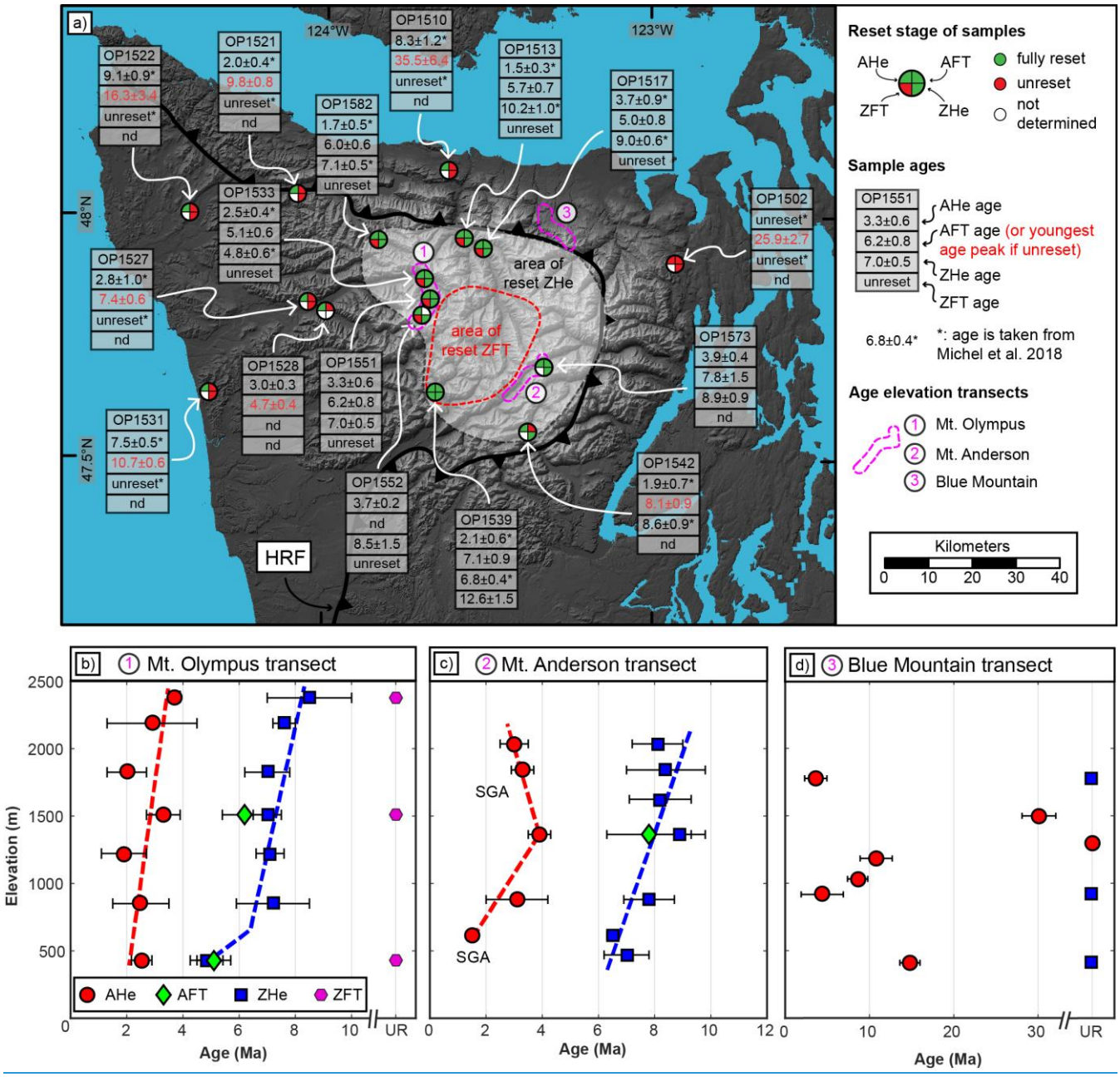

Figure 4: a) Map of samples, for which three to four different thermochronometer systems are available. The pie charts show the reset stage of a particular thermochronometer system for the sample. If AFT ages are unreset, the peak age of the youngest age population is given as sample age (see Table 3 for older populations). Ages denoted with an asterisk are taken from Michel et al. (2018). The Hurricane Ridge Fault (HRF) separates the rocks of the accretionary wedge from the surrounding Coast Range Terrane in the hanging wall. The locations of the three different elevation transects (Mt. Olympus, Mt. Anderson and Blue Mountain) are indicated on the map and the resulting age-elevation plots are shown in b) to d). In b) and c) the dashed coloured lines correspond to possible exhumation rates interpreted from the respective thermochronometer. All uncertainties are 1 standard deviation, SGA = single-grain age.

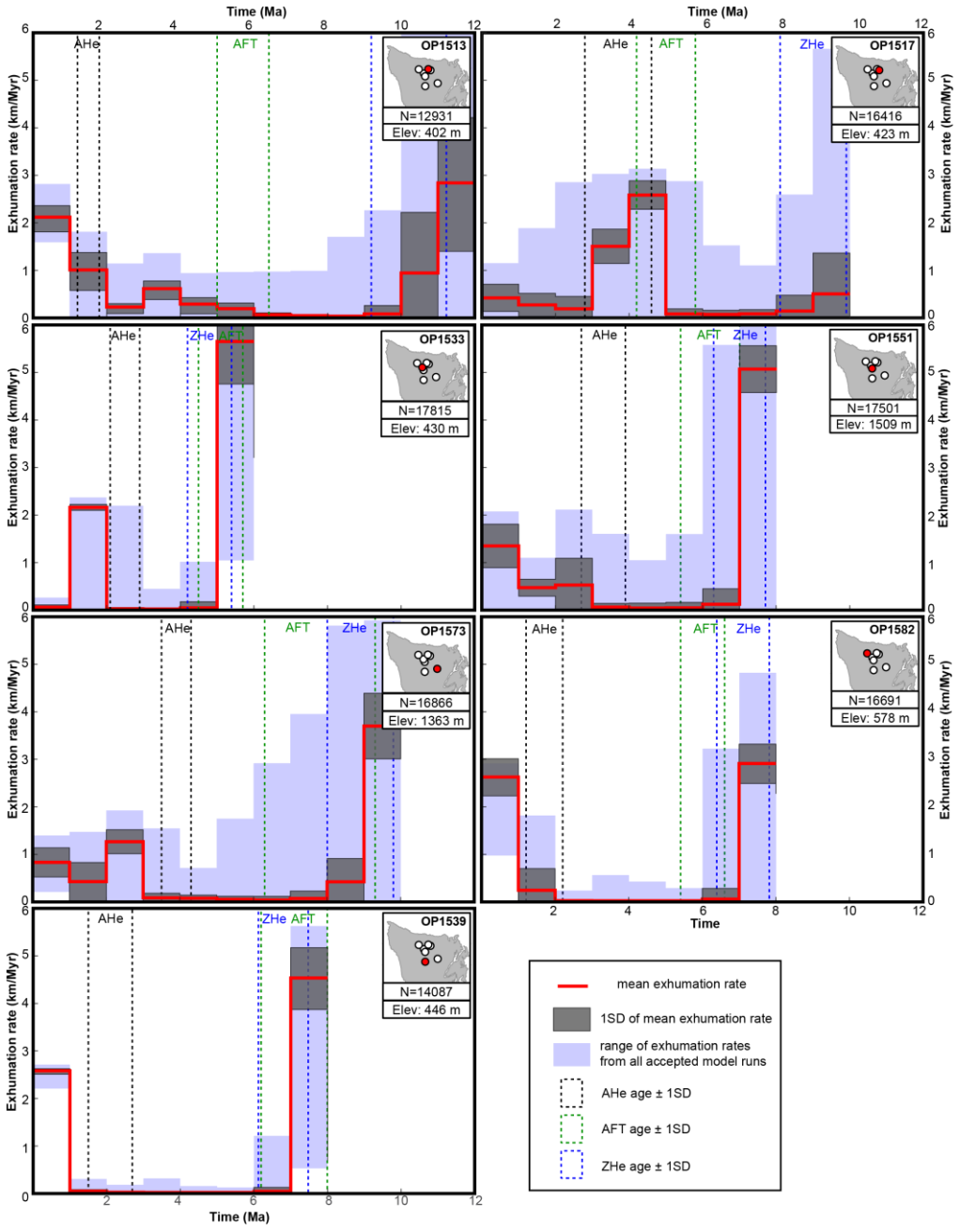

Figure 5: Results from the thermo-kinematic Monte Carlo modelling for the seven considered samples (OP1513, OP1517, OP1533, OP1539, OP1551, OP1573, OP1582). Location of each sample within the Olympic Peninsula is shown, together with the respective elevation (Elev). The entire range of exhumation rates from the number of accepted model runs (N) is outlined by the blue shaded area, from which the mean rate and one standard deviation (1SD) is calculated at each time step. Black, green, and blue stippled boxes outline measured AHe, AFT, and ZHe ages of the samples with 1SD.

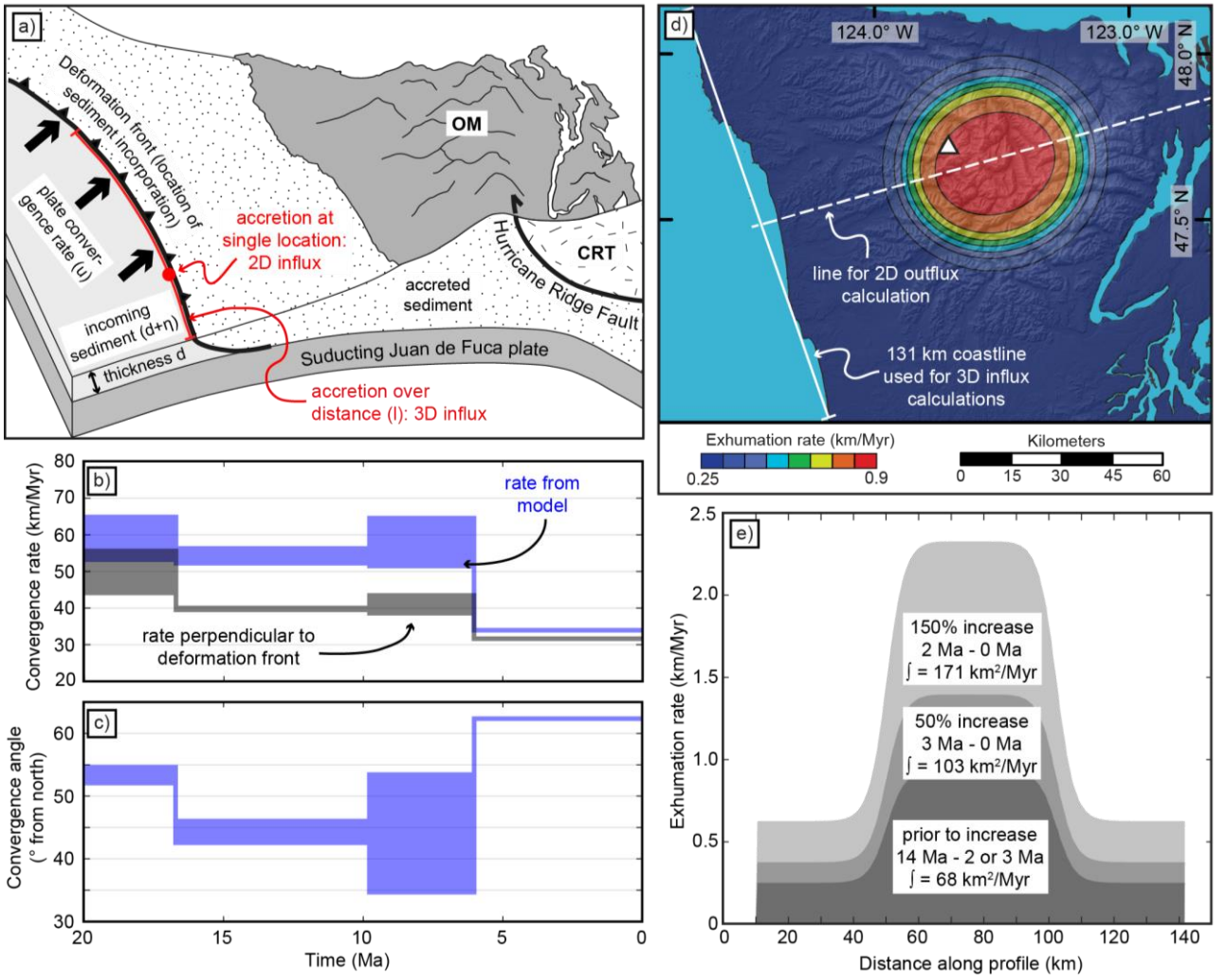

Figure 6: Constraints used for our quantitative accretionary influx and denudational outflux calculations. a) Cartoon illustrating our approach for calculating the accretionary influx. The influx corresponds to the sediment scraped off from the subducting Juan de Fuca Plate, and is governed by the plate convergence rate (u) and the incoming sediment properties (thickness d, porosity η). We discern a two-dimensional geometry, where sediment is accreted at a single location within a vertical column at the deformation front, and a three-dimensional geometry, where accretion is considered along a length (l) within a vertical plane. This length corresponds to the length of the coastline indicated in panel (d). OM = Olympic Mountains, CRT = Coast Range Terrane. b) Temporal evolution of the plate convergence rate used in the calculations, considering only the component perpendicular to the deformation front (black envelope), and the original output (blue envelope) from the plate reconstruction model of Doubrovine and Tarduno (2008). To provide an uncertainty for our calculations, we consider a range of convergence rates (comprising the width of the envelope) for each time step, based on two different rotation models in the model of Doubrovine and Tarduno (2008) (see text for details). c) Temporal evolution of the plate convergence angle (Doubrovine and Tarduno, 2008) used to correct the plate convergence rate in b). d) Exhumation rate pattern from Michel et al. (2018) used for our outflux calculations. The range of displayed rates (0.25–0.9 km/Ma) corresponds to the rates prior to the glacially induced increase in exhumation rates. In the two-dimensional scenario, we integrate the exhumation rates along the dashed line. In the three-dimensional scenario, we integrate over the entire pattern. e) Exhumation rates along dashed line shown in d) and the resulting value of the integral, prior to the glacially induced increase in rates, for a 50% increase and a 150% increase. The duration over which the respective integral is applied is indicated as well.

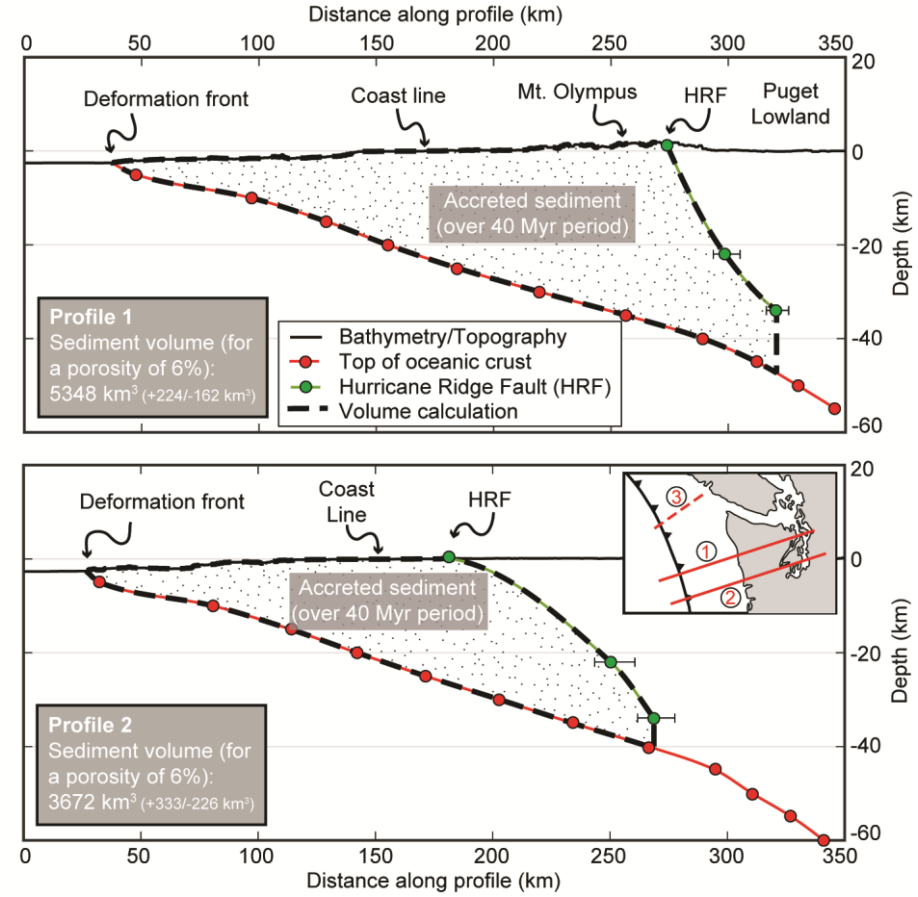

Figure 7: Sediment volumes calculated along two cross-sections spanning the Olympic Peninsula (Profile 1 and 2, vertical exaggeration=2, see inset for location). For explanation of the used procedure see text. The reported uncertainties for the volume are based on the uncertainties in the position of the Hurricane Ridge Fault (indicated with error bars at the respective symbol). Numbers in inset correspond to (1) = position of Profile 1, (2) = position of Profile 2, (3) = position of profile by Davis and Hyndman (1989), referred to in the text.

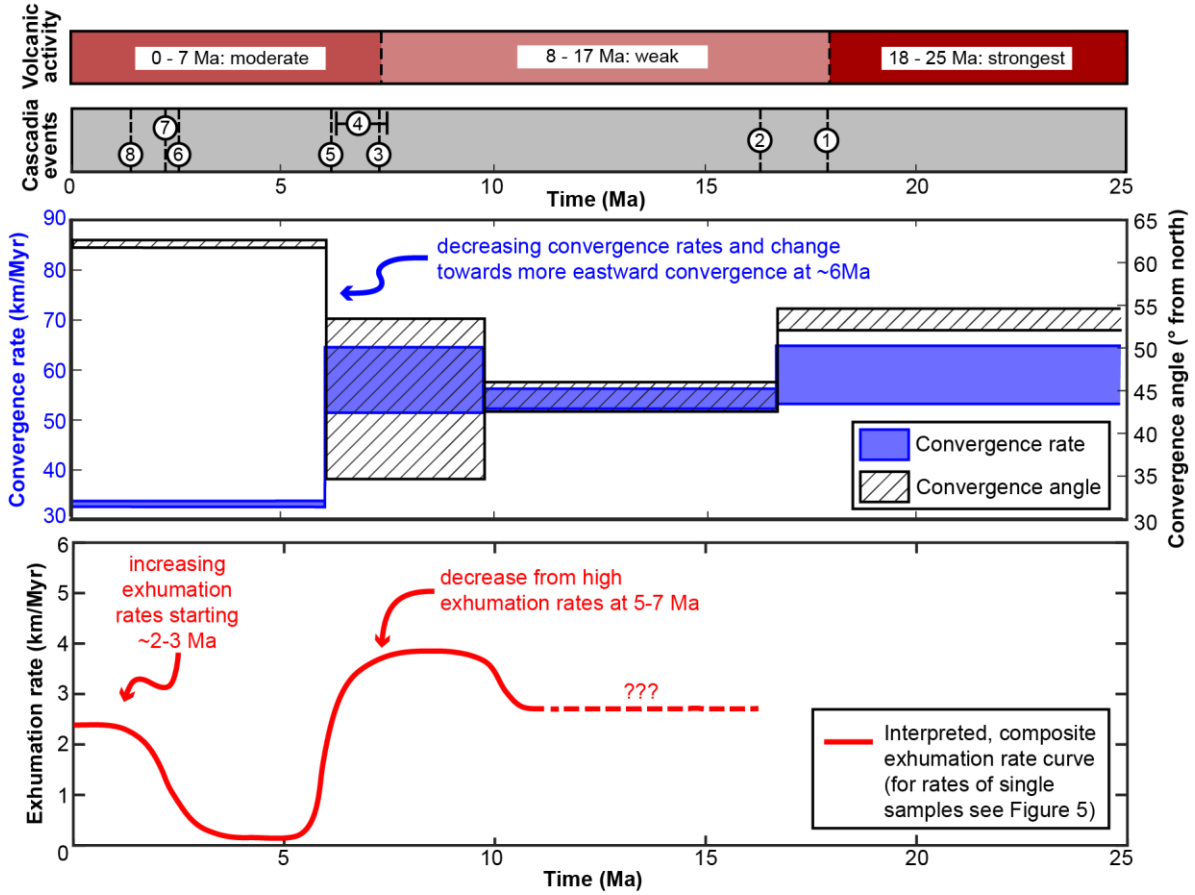

Figure 8: Summary of volcanic activity, tectonic and climatic events, and convergence rate and angle at the Cascadia Subduction Zone in comparison with our interpreted exhumation rates for the past 25 Myr. Exhumation rates are limited to the time interval covered by our thermochronometric ages (0–11 Ma). The curve depicts the interpreted evolution of exhumation rates, based on the modelling results shown in Figure 5 (see text for details). Volcanic activity after du Bray and John (2011). Tectonic and climatic events are (1) start of exhumation of the Olympic Mountains (Brandon et al., 1998), (2) onset of uplift of the Oregon Coast Range (McNeill et al., 2000), (3) rotation in stress field (Priest, 1990), (4) faster uplift in Oregon Coast Range (McNeill et al., 2000), (5) Pacific-wide plate reorganization (Wilson, 2002), (6) onset of North American glaciation (Haug et al., 2005), (7) onset of glaciation within the Olympic Mountains (Easterbrook, 1986), (8) change in the deformational style of the offshore accretionary wedge (Flueh et al., 1998). Convergence rate and angle from Doubrovine and Tarduno (2008).

Table 1: Data for the ocean drill cores shown in Fig. 3.

Core	**ODP 888**	**OPD 1027**	**DSDP 174**
Drilled/total sediment thickness[a] (m)	570/2600	620/620	880/910
Cored Quaternary sediment (m)	570	460	430[b]
Maximum age of Quaternary sediments[c] (Ma)	0.6	1.7	1.7
Amount of Quaternary section of total core (%)	-	74	47
Age of oceanic crust[d] (Ma)	6.5	3.2	7.5
Quaternary sedimentation rate (m/Myr)	950[e]	270	250
Pre-Quaternary/total sedimentation rate[f] (m/Myr)	-/400	110/190	80/120

Notes: For core ODP 888, information is taken from Westbrook et al. (1994), for ODP 1027 from Su et al. (2000), and for DSDP 174 from Kulm et al. (1973). Sedimentation rates are calculated in this study using the reported thicknesses and age constraints.

[a]: If total thickness exceeds drilled thickness, then the total thickness was estimated from seismic data (e.g., ODP 888).

[b]: Due to poor core recovery, the Plio-Pleistocene boundary can only be confined to be between 418 and 446 m.

[c]: Ages based on biostratigraphy. For cores ODP 1027 and DSDP 174, the Plio-Pleistocene boundary was recovered and an age of 1.7 Ma is used here as reported by Su et al. (2000).

[d]: For cores ODP 888 and DSDP 174, the age refers to the age of the oceanic crust and is taken from Figure 3 at the respective location of the core. For ODP 1027, the age refers to the age of the oldest sediment in the core taken from Su et al. (2000).

[e]: This rate is calculated for the recovered core interval, which only encompasses 600 ka.

[f]: Total sedimentation rate = total thickness divided by age of oceanic crust.

Table 2: Coordinates, elevations, and thermochronometric cooling ages for samples considered in this study.

Sample	Latitude (°)	Longitude (°)	Elevation (m)	AHe ± 1SD (Ma)	AFT ± 1SD (Ma)	ZHe ± 1 SD (Ma)	ZFT ± 1SD (Ma)
Mount Olympus transect samples							
OP1533[a]	*47.87572*	*-123.69427*	*430*	*2.5 ± 0.4*	*5.1* ± 0.6	*4.8* ± 0.6	*unreset*
OP1550	47.81568	-123.69601	1825	2.0 ± 0.7	nd	7.0 ± 0.8	nd
OP1551	*47.82647*	*-123.68324*	*1509*	*3.3 ± 0.6*	*6.2 ± 0.8*	*7.0 ± 0.5*	*unreset*
OP1552	47.80155	-123.71102	2377	3.7 ± 0.2	nd	8.5 ± 1.5	unreset
OP1553	47.80377	-123.70244	2188	2.9 ± 1.6	nd	7.6 ± 0.4	nd
OP1554	47.83979	-123.69330	1222	1.9 ± 0.8	nd	7.1 ± 0.5	nd
OP1555	47.85457	-123.69194	851	2.5 ± 1.0	nd	7.2 ± 1.3	nd
Blue Mountain transect samples							
OP1548[a]	48.02186	-123.34295	410	14.8 ± 1.2	nd	unreset	nd
OP1557	47.98098	-123.31173	917	4.4 ± 2.5	nd	nd	nd
OP1558	47.97233	-123.30092	1032	8.6 ± 1.2	nd	unreset	nd
OP1559	47.97287	-123.28636	1184	10.8 ± 1.9	nd	nd	nd
OP1560	47.96709	-123.27110	1324	unreset	nd	nd	nd
OP1561	47.95783	-123.26785	1500	30.1 ± 2.0	nd	nd	nd
OP1562	47.95696	-123.26078	1778	3.6 ± 1.3	nd	unreset	nd
Mount Anderson transect samples							
OP1570	47.70483	-123.32813	1624	nd	nd	8.2 ± 1.1	nd
OP1571	47.71657	-123.32927	2035	3.0 ± 0.5	nd	8.1 ± 0.9	nd
OP1572[b]	47.71473	-123.32815	1842	3.3 ± 0.4	nd	8.4 ± 1.4	nd
OP1573	*47.69400*	*-123.32765*	*1363*	*3.9 ± 0.4*	*7.8 ± 1.5*	*8.9 ± 0.9*	*nd*
OP1574	47.68899	-123.35093	881	3.1 ± 1.1	nd	7.8 ± 0.9	nd
OP1576[b]	47.67451	-123.39235	614	1.5 ± 0.2	nd	6.5 ± 0.2	nd
OP1577	47.64185	-123.43398	470	nd	nd	7.0 ± 0.8	nd
Equal-elevation samples							
OP1502[a]	47.90796	-122.92804	325	unreset	unreset	unreset	nd
OP1510[a]	48.09852	-123.62231	273	8.3 ± 1.2	unreset	unreset	nd

OP1513[a]	*47.96015*	*-123.57273*	*402*	*1.5 ± 0.3*	*5.7 ± 0.7*	*10.2 ± 1.0*	*unreset*
OP1517[a]	*47.93891*	*-123.51376*	*423*	*3.7 ± 0.9*	*5.0 ± 0.8*	*9.0 ± 0.6*	*unreset*
OP1521[a]	48.04832	-124.08702	390	2.0 ± 0.4	unreset	unreset	nd
OP1522[a]	48.00530	-124.41620	367	9.1 ± 0.9	unreset	unreset	nd
OP1527[a]	47.82500	-124.05184	280	2.8 ± 1.0	unreset	unreset	nd
OP1528	47.80681	-123.99661	140	3.0 ± 0.3	unreset	nd	nd
OP1529[a]	47.78265	-124.14257	343	6.2 ± 1.1	unreset	unreset	nd
OP1531[a]	47.63659	-124.34966	50	7.5 ± 0.5	unreset	unreset	nd
OP1539[a]	*47.64151*	*-123.65870*	*446*	*2.1 ± 0.6*	*7.1 ± 0.9*	*6.8 ± 0.4*	*12.6 ± 1.5*
OP1542[a]	47.56001	-123.37533	450	1.9 ± 0.7	unreset	8.6 ± 0.9	nd
OP1556	48.00848	-123.89398	470	3.3 ± 0.9	nd	nd	nd
OP1582[a]	*47.95595*	*-123.83732*	*578*	*1.7 ± 0.5*	*6.0 ± 0.6*	*7.1 ± 0.5*	*unreset*

Notes: Samples in italics are used for 1D thermo-kinematic modelling. Results from single-grain analyses for AHe and ZHe are reported in Tables S1 and S2, respectively. Further details for AFT and ZFT dating can be found in Table 3, and single-grain analyses for apatite and zircon are reported in Tables S3 and S4, respectively. 1SD = one standard deviation, nd = not determined.

[a]: AHe and ZHe ages of the respective samples are from Michel et al. (2018).

[b]: Reported sample AHe ages are single-grain ages, because the yield of suitable apatite grains did not allow to date more grains.

Table 3: Results from fission-track dating.

Reset samples

Sample +Mineral	Grain ages (Ma)	χ^2 (%)	N	reset state	Sample age ± 1SD (Ma)
OP1513 ap	0.9–17	47	24	R	5.7 ± 0.7
OP1517 ap	0–13	25	17	R	5.0 ± 0.8
OP1533 ap	2–15	11	20	R	5.1 ± 0.6
OP1539 ap	3–31	21	21	R	7.1 ± 0.9
OP1539 zr	8–18	19	21	R	12.6 ± 1.5
OP1551 ap	0–16	76	21	R	6.2 ± 0.8
OP1573 ap	5–17	11	6	R	7.8 ± 1.5
OP1582 ap	0–19	55	22	R	6.0 ± 0.6

Notes: For AFT and ZFT, 20 grains per sample were dated in a first step and it was checked whether the sample passes the χ^2-test and can be considered as reset (i.e., > 5%; an indication for belonging to the same age population, e.g., Galbraith, 2005). If so, the pooled ζ-age was considered as the sample age and reported here. If a sample failed the χ^2-test (i.e., < 5%), the sample is considered unreset and, in the case of AFT, 100 grains were dated if enough grains are available. The detrital age distribution was then decomposed into detrital age populations using BINOMFIT (Brandon, 1992, 1996) and the peak ages of those populations (with asymmetric error range for each age peak, corresponding to the 68% confidence interval, CI) are reported. For the ZFT method, the information whether the sample is reset or unreset is sufficient for this study and no further grains were dated. Fraction equals the amount of grains contained within the respective age peak. N=number of counted grains. Contrary to Brandon et al. (1998) we did not consider multiply or partially reset AFT samples but treated them as unreset, because our thermo-kinematic model can only be applied to fully reset samples.

[a]: Results for this sample are obtained by merging grains from our sample OP1527 (n=103) and sample AR39 (n=31) from Brandon et al. (1998).

Unreset samples

Sample +Mineral	Grain ages (Ma)	χ^2 (%)	N	reset state	Age peaks of the age populations: Age (Ma)	68% CI (Ma)		Fraction (%)	Age (Ma)	68% CI (Ma)		Fraction (%)	Age (Ma)	68% CI (Ma)		Fraction (%)
OP1502 ap	10–630	0	94	UR	25.9	-2.5	+2.7	29.4	84.7	-8.1	+9.0	48.3	243	-54.6	+70.0	22.2
OP1510 ap	18–191	0	80	UR	35.5	-5.4	+6.4	34.5	52.6	-6.0	+6.8	52.9	100.3	-23.6	+30.7	12.6
OP1513 zr	17–82	0	23	UR	30.9	-3.5	+4.0	70.9	52.6	-7.5	+8.8	29.1	-	-	-	-
OP1517 zr	27–57	0	25	UR	33.7	-8.0	+10.5	15.5	41.4	-4.5	+5.1	84.5	-	-	-	-
OP1521 ap	0.5–499	0	103	UR	9.8	-0.8	+0.8	60.5	35.1	-4.0	+4.5	30.6	261.9	-50.4	+62.2	8.9
OP1522 ap	6–237	0	20	UR	16.3	-2.8	+3.4	20.2	41.8	-3.5	+3.8	59.7	130.1	-32.7	+43.5	20
OP1527[a] ap	1–992	0	134	UR	7.4	-0.5	+0.6	67.7	24.0	-2.0	+2.2	28.0	209.3	-65.4	+94.5	3.5
OP1528[b] ap	0.4–237	0	80	UR	4.7	-0.4	+0.4	75.7	14.6	-2.2	+2.5	24.1	-	-	-	-
OP1531 ap	6–684	0	100	UR	10.7	-0.5	+0.6	50.6	30.2	-1.8	+1.9	40.1	149.0	-21.7	+25.3	6.5
OP1533 zr	29–106	0	23	UR	35.6	-4.0	+4.5	43.5	53.5	-5.7	+6.4	47.7	95.8	-12.5	+14.3	8.7
OP1542 ap	3–43	0	19	UR	8.1	-0.8	+0.9	77.1	27.9	-3.6	+4.2	22.9	-	-	-	-

OP1551 zr	9–57	0	23	UR	15.1	-1.8	+2.0	62.7	25.5	-3.6	+4.1	21.0	49.9	-6.5	+7.4	16.3
OP1552 zr	10–38	0	24	UR	14.0	-1.5	+1.7	79.7	32.3	-3.7	+4.2	20.3	-	-	-	-
OP1582 zr	28–68	0	23	UR	31.1	-3.5	+3.9	35.0	52.1	-5.5	+6.2	65.0	-	-	-	-

Table 4: List of parameters used for the Pecube modelling.

Parameter	Value	Source
Thermal conductivity	1.83 W $m^{-1}K^{-1}$	average value for six drill cores in sediment material in the shelf offshore from Vancouver Island (Lewis et al., 1988)
Specific heat capacity	1200 J $kg^{-1}K^{-1}$	
Crustal density	2700 kg m^{-3}	
Mantle density	3200 kg m^{-3}	
Temperature at the base of the model	400 °C	extrapolation to greater depths from temperature estimates based on heat flow measurements on the shelf (Hyndman et al., 1990; Hyndman and Wang, 1993; Booth-Rea et al., 2008)
Temperature at sea level	8 °C	
Atmospheric lapse rate	6.69 °C km^{-1}	
Crustal heat production	0.77 µW m^{-3}	average value from drill cores on the shelf offshore Vancouver Island (Lewis and Bentkowski, 1988)
Model depth	20 km	minimum thickness of the accretionary wedge below the Olympic Mountains (e.g., Davis and Hyndman, 1989)

Table 5: Results from influx and outflux calculations for both two-dimensional (2D) and three-dimensional (3D) geometries.

	Accretionary influx over 14 Myr period			Denudational outflux over 14 Myr period		
	Minimum [a] (1.5 km)	Maximum [a] (2.5 km)	Increase at 2 Ma [a] (1.5 → 2.5 km)	Constant rates [b]	50% increase at 3 Ma [b]	150% increase at 2 Ma [b]
2D[c]	520–540 km^3	980–1020 km^3	580–600 km^3	960 km^3	1060 km^3	1160 km^3
3D	68–71 x 10^3 km^3	128–133 x 10^3 km^3	75–78 x 10^3 km^3	72 x 10^3 km^3	80 x 10^3 km^3	88 x 10^3 km^3

Notes:

[a]: Sensitivity to incoming sediment thickness: The accretionary influx volume is calculated for three different sediment thicknesses, yielding a minimum volume (1.5 km thickness), maximum volume (2.5 km thickness), and a more realistic volume (where the volume increases from 1.5 km to 2.5 km at 2 Ma).

[b]: Sensitivity to an increase in exhumation rates: The denudational outflux volume is calculated assuming constant exhumation rates, and considering the increase in exhumation rates due to glacial erosion, with an increase by 50% at 3 Ma or an increase by 150% at 2 Ma. Exhumation rates are based on Michel et al. (2018) and displayed in Figs. 6d and e.

[c]: Strictly speaking, the volumes calculated for the 2D scenarios have units of km^2 or km^3 per km of width/depth (of either influx or outflux). However, to not confuse the reader when we talk of volumes, we decided to use the unit km^3, which does not change the actual value, but only the unit of the respective calculated volume.